National Center for Asphalt Technology
NCAT
at AUBURN UNIVERSITY

NCAT Report 25-01

November 2025

Determining Structural Layer Coefficient and Comparative Life Cycle Assessment for Asphalt Mixtures with HiMA™ Technology

Suri Gatiganti, David Timm, Nam Tran, Samina Samrose, and Lorena Garcia Cucalon

HiMA is a trademark of Kraton Corporation

Determining Structural Layer Coefficient and Comparative Life Cycle Assessment for Highly Modified Asphalt (HiMA) Mixtures

By

Suri Gatiganti, PhD
Assistant Research Professor
National Center for Asphalt Technology
Auburn University, Auburn, Alabama

David Timm, PhD
Elton & Lois Huff Eminent Chair Professor
Department of Civil and Environmental Engineering
Auburn University, Auburn, Alabama

Nam Tran, PhD
Associate Director and Research Professor
National Center for Asphalt Technology
Auburn University, Auburn, Alabama

Samina Samrose
Graduate Research Assistant
National Center for Asphalt Technology
Auburn University, Auburn, Alabama

Lorena Garcia Cucalon, PhD
Sales Manager
Kraton Corporation, Houston, Texas

November 2025

TABLE OF CONTENTS

LIST OF FIGURES

LIST OF TABLES

CHAPTER 1: INTRODUCTION

Asphalt pavements are vital for transportation infrastructure, providing a smooth, durable surface for the public. Each year, state departments of transportation (DOTs) spend significant resources to maintain these networks, addressing the impact of traffic, climate, and aging on pavement performance. As traffic continues to increase, coupled with climate change, these impacts are even more severe on asphalt pavements, leading to concerns over durability and service life. To address these issues, high polymer asphalt binder grades such as Kraton's HiMA™ technology have emerged as an effective solution to enhance the performance of asphalt mixtures and pavements.

The purpose of the research presented in this report was to assess the contribution of HiMA mixtures to strengthen pavement structures and reduce environmental impacts through enhanced performance. The findings can be a valuable resource for engineers, researchers, and practitioners involved in designing asphalt pavements using the 1993 American Association of State Highway and Transportation Officials (AASHTO) Design Guide and evaluating the benefits of using HiMA mixtures [1].

Based on data from three experiments conducted at the National Center for Asphalt Technology (NCAT) Test Track, the structural contribution of HiMA mixtures was determined using the structural layer coefficient concept. Four approaches were used to analyze the structural layer coefficients of HiMA mixtures in these experiments, and the results are presented in Chapter 2.

In addition, comparative life cycle assessments (LCAs) were conducted on two test sections, one with a conventional asphalt mixture and the other with a HiMA-modified mixture, constructed in the 2009 Test Track research cycle. The LCAs were conducted for two scenarios, cradle-to-constructed and cradle-to-grave boundaries. The results of these assessments are presented in Chapter 3. Finally, the key findings from the prior analyses are summarized in Chapter 4, along with conclusions and recommendations for implementation.

CHAPTER 2: STRUCTURAL LAYER COEFFICIENT OF HIMA MIXTURES

2.1 INTRODUCTION

Structural layer coefficients are critical to the 1993 AASHTO Design Guide of flexible pavements because they factor directly into the thickness computation of the layers within the pavement cross section [1]. This design method is commonly used by state departments of transportation across the U.S. for both flexible and rigid pavement design, and accurate structural layer coefficients are needed for the proper utilization of any material within the design system. This is especially true of newly developed innovative materials, such as HiMA, since using default structural layer coefficients developed for other materials may not capture the properties of the new material, resulting in non-optimal designs.

Within the 1993 AASHTO Guide [1] design system, the structural coefficients of layers are multiplied by their corresponding layer thicknesses to produce a structural number (SN). The sum of these products, including all the layers in the cross section, must equal or exceed the required SN for the pavement cross section. The required SN is determined from a regression equation that accounts for the soil support, reliability, variability, traffic, and expected performance of the section. Therefore, thicknesses that provide the necessary SN are computed, given a set of structural layer coefficients representing each layer.

Structural layer coefficients were first introduced at the conclusion of the AASHO Road Test and were derived from statistically fitted observed pavement performance to the pavement cross sections in various test loops at the Road Test [2]. As listed in Table 2.1, structural layer coefficient values for asphalt concrete (AC) ranged from 0.33 up to 0.83, depending on the test loop. These values, taken individually, have no inherent meaning. However, when compared with each other or to those of other materials, they represent the relative structural contribution made by a particular material relative to other materials. For example, the most commonly-used structural layer coefficient in the U.S. is 0.44 for asphalt materials, which appears several times in Table 2.1. A commonly-used value for aggregate base is 0.15. Dividing these two values (0.44/0.15 = 2.93) produces an understanding of the structural equivalency between asphalt and aggregate base (i.e., 1 inch of asphalt is worth about 3 inches of aggregate base).

Table 2.1 Asphalt Structural Layer Coefficients from AASHO Road Test [2]

Loop	Layer Coefficient (a_1)	Test Sections	R^2
2	0.83	44	0.80
3	0.44	60	0.83
4	0.44	60	0.90
5	0.47	60	0.92
6	0.33	60	0.81

Since structural layer coefficients factor directly into thickness design, there is a great need to develop them for new or innovative materials, as mentioned above. Therefore, methods of calibration have been developed and are well documented [3]. One such recalibration effort was conducted at NCAT to recalibrate structural layer coefficients used by the Alabama Department of Transportation (ALDOT) using Test Track data [4]. The study utilized field-measured performance data and backcalculated AC moduli to recommend increasing the layer coefficient for ALDOT from 0.44 to 0.54. This increase reflects the improved performance of modern materials used by ALDOT and results in an 18.5% reduction in pavement design thickness.

Like all new or innovative asphalt materials, there is a need to have a calibrated structural layer coefficient for HiMA-modified asphalt concrete. Without a calibrated structural layer coefficient, designers are relegated to assuming a value which may lead to non-optimal designs (i.e., over- or under-conservative). Fortunately, sections have been built and fully tested at the NCAT Test Track with HiMA, which facilitates applying various calibration approaches to compute structural layer coefficients, as documented in the remainder of this chapter.

2.2 OBJECTIVE

Given the need described above, the objective of this investigation was to develop a recommended structural layer coefficient for asphalt concrete modified with HiMA.

2.3 SCOPE OF WORK

To accomplish the objective, this investigation utilized test sections built in three different test cycles at the NCAT Test Track. The 2009 sections included a control and a HiMA-modified section. The 2010 section was part of a HiMA rehabilitation at the Test Track. The 2015 sections included another control and HiMA-modified sections. The procedures used to compute structural layer coefficients varied depending on the availability of requisite data sets for each section but included computing effective structural numbers (SNeff), correlating structural layer coefficients to in situ modulus, determining equivalent sections from strain response and lab fatigue performance data, and utilizing field performance data. The following sections detail the cross sections, methodologies, and data and conclude with a recommended structural layer coefficient for HiMA-modified asphalt concrete.

2.4 TEST FACILITY & SECTIONS

The NCAT Test Track, shown in Figure 2.1, is a 1.7-mile closed loop pavement research facility that enables full-scale evaluation of flexible pavement systems. Located near Auburn University in east-central Alabama, the Test Track consists of forty-six 200 ft test sections that are loaded with triple-trailer vehicles (Figure 2.2) operating at 45 mph. Each truck applies about 12.8 equivalent standard axle loads (ESALs) per pass, and the fleet accumulates approximately 10 million equivalent single axle loads (MESALs) in two years of trafficking. The Test Track operates on three-year cycles where traffic is applied for two years, with forensic work and reconstruction of the track conducted every third year. Sections are numbered according to their tangent (N = north; S = south) and their sequential number in the tangent. As described below, the sections for this investigation were built in different research cycles.

Figure 2.1 NCAT Test Track.

Figure 2.2 NCAT Test Track Triple-Trailer Truck (12.8 ESAL/vehicle).

2.4.1 2009 Test Sections

The two sections built in the 2009 research cycle were designed to compare an asphalt mix modified with HiMA (N7-HiMA) to a control section (S9-Control) modified with a more typical percentage of polymer modification. These sections were left in place through two test cycles with approximately 20 MESALs applied by the end of 2014. Both sections were built on the same Test Track subgrade and crushed granite aggregate base. However, the design AC thickness of N7-HiMA was 1.25 inches thinner than S9-Control to demonstrate the expected superior cracking resistance of the HiMA-modified mix. The as-built cross-sections are shown in Figure 2.3, where the thicknesses represent section-wide average depths obtained from 12 locations in each section measured with a total station. The top three layers in each section are asphalt concrete, with the next two layers being the aggregate base and subgrade, respectively. Table 2.2 contains the mix design parameters for each asphalt lift, while Table 2.3 shows the as-built asphalt properties. Note that N7-HiMA contained a 7.5% Styrene-butadiene-styrene (SBS) polymer modified binder in all three lifts, while S9-Control contained a 2.8% SBS polymer modified binder in the upper two lifts and an unmodified binder in the base lift. As documented previously [4], two design gradations were used in this study. The surface layers utilized a 9.5 mm nominal maximum aggregate size (NMAS) dense gradation, while the intermediate and base mixtures used a 19 mm NMAS dense gradation. The aggregate gradations were a blend of granite, limestone, and sand using locally available materials. Distinct gradations were developed for each control mixture (surface, intermediate, and base) to achieve the necessary volumetric targets as the binder grade and nominal maximum aggregate size (NMAS) changed between layers. The HiMA gradations used in section N7-HiMA were very similar to the control mixtures used in section S9. More details regarding these sections have been previously documented [5, 6].

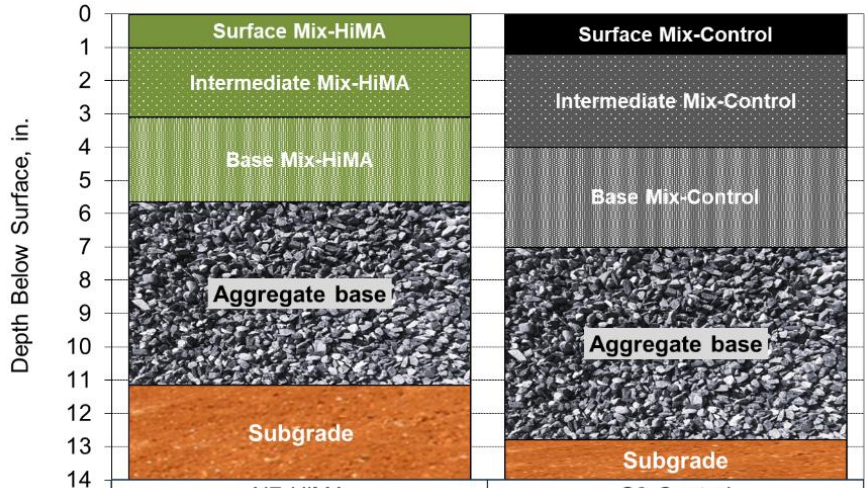

	N7-HiMA	S9-Control
Subgrade	Infinite	Infinite
Aggregate Base	5.52	5.80
Base Mix	2.55	3.01
Intermediate Mix	2.09	2.78
Surface Mix	1.01	1.22

Figure 2.3 2009 Test Sections (data in the table are thicknesses of each layer in inches).

Table 2.2 2009 Mix Design Parameters [5]

Mixture Type	N7-HiMA		S9-Control		
Lift (1=surface; 2=intermediate, 3=base)	1	2 & 3	1	2	3
Asphalt PG Grade	88-22	88-22	76-22	76-22	67-22
Nominal Max. Aggregate Size (NMAS), mm	9.5	19	9.5	19	19
% Polymer Modification	7.5	7.5	2.8	2.8	0
Design Air Voids (VTM), %	4.0	4.0	4.0	4.0	4.0
Total Combined Binder (P_b), % wt	5.9	4.6	5.8	4.7	4.6
Effective Binder (P_{be}), %	5.3	4.2	5.1	4.1	4.1
Dust Proportion (DP)	1.1	0.9	1.1	0.9	1.1
Maximum Specific Gravity (G_{mm})	2.474	2.570	2.483	2.575	2.574
Voids in Mineral Aggregate (VMA), %	16.2	14.0	15.8	13.9	13.9
Voids Filled with Asphalt (VFA), %	75	72	75	71	71

Table 2.3 2009 As-Built Mix Parameters [6]

Lift	Surface		Intermediate		Base	
Section	N7-HiMA	S9-Control	N7-HiMA	S9-Control	N7-HiMA	S9-Control
NMAS, mm	9.5	9.5	19.0	19.0	19.0	19.0
%SBS	7.5	2.8	7.5	2.8	7.5	0.0
PG Grade	88-22	76-22	88-22	76-22	88-22	67-22
Asphalt Content, %	6.3	6.1	4.6	4.4	4.6	4.7
Air Voids, %	6.3	6.9	7.3	7.2	7.2	7.4
Mix Temp, °F	345	335	345	335	340	325
Comp. Temp, °F	297	275	247	273	240	243

2.4.2 2010 Rehabilitation using HiMA

Computing a structural layer coefficient from the Test Track section that was rehabilitated using HiMA in 2010 requires an understanding of the original section that was built in 2006 for the Oklahoma DOT (ODOT). Figure 2.4 shows the design thicknesses and materials of the original section (Section N8), which was followed by the first mill and inlay using conventional materials after the first 10 MESALs, which was then followed by another mill and inlay using HiMA after another 4.5 MESALs. At the time of the HiMA rehabilitation, the material was referred to as a high polymer mix (HPM).

As documented previously [7], "Section N8 was the thinner of two test sections sponsored by ODOT in the 2006 research cycle to study the perpetual pavement thickness design concept. The original stiff Test Track subgrade under these two sections was excavated to a depth of 4 feet and replaced with a soft subgrade that was more representative of roadway soils in Oklahoma. The top 8 inches of the imported soft subgrade was replaced with the same stiff material that had been removed to simulate lime stabilization. As seen in Figure 2.4, Section N8 had a total AC thickness of 10 inches, consisting of a 2-inch rich bottom layer, 6 inches of dense Superpave mix, and 2 inches of stone matrix asphalt (SMA) surface mix. The rich-bottom layer mixture had a higher binder content to achieve 2% design air voids, instead of the typical 4% design air voids in a Superpave mix design. Information on the design, production, and placement of all the layers in both sections has been previously documented [8, 9, 10]. Roughness began to increase in Section N8 near the end of the 2006 research cycle after approximately 7 million ESALs. Cracking first reached the surface after 8.3 million ESALs, and the section needed rehabilitation by the end of the 2006 cycle (i.e., 10 million ESALs)."

Before beginning the next test cycle in 2009, the section was rehabilitated with a mill-and-inlay approach to a depth of 5 inches, and a fabric interlayer was placed between the new SMA and Superpave layers. This approach was at the direction of ODOT and was considered standard practice at the time. Cracking was evident on the milled surface before inlay, and the pavement only survived another 3.5 MESALs during the 2009 cycle before needing another rehabilitation, which occurred in 2010.

Since the first rehabilitation failed so quickly, it was decided to take a more aggressive approach in the next rehabilitation of N8 in 2010. The adjacent section (N7) described above and shown in Figure 2.3 was performing very well, and it was decided to use HiMA to rehabilitate N8 with the expectation that the enhanced cracking resistance would help mitigate reflection cracking from the underlying distressed pavement. The distressed pavement was milled to a depth of 5.75 inches and replaced with HiMA in three

lifts, as shown in Figure 2.4. The HiMA mixtures were designed with a 7.5% SBS polymer modified binder, and the bottom layer was designed to lower design air voids to achieve a richer bottom to enhance the cracking resistance further. Table 2.4 lists the as-built properties of the HiMA mixes used in the rehabilitation.

After rehabilitation with HiMA, the section did markedly better than the original and first rehabilitation in terms of cracking, rutting, and roughness. It was left in place for the remaining duration of the 2009 test cycle and continued into the following 2012 cycle, accumulating approximately 15 MESALs with excellent performance throughout, though it did experience some increase in roughness, which allowed for calibration to actual performance as described below.

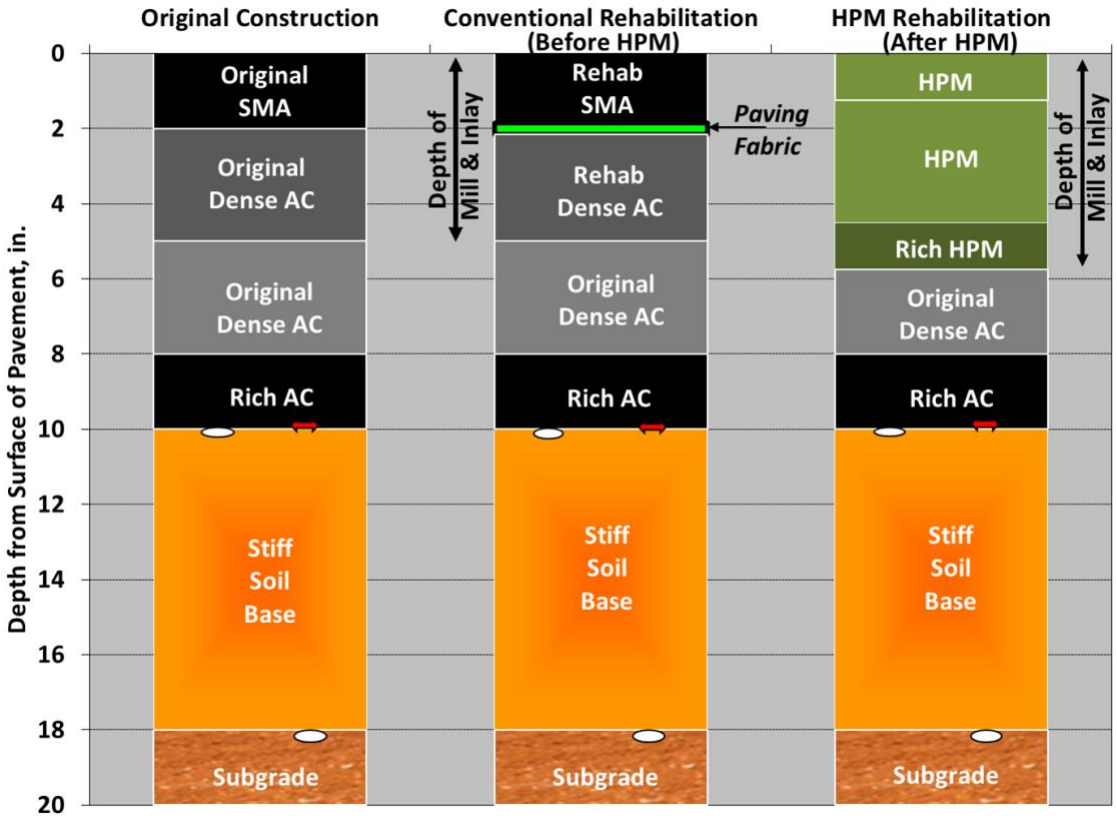

Figure 2.4 2010 Rehabilitation Cross Sections [7].

Table 2.4 2010 HiMA Rehabilitation Properties

HiMA Layer	Surface	Binder	Base
SBS, %	7.5	7.5	7.5
NMAS, mm	9.5	19	9.5
Asphalt Content, %	5.9	4.8	6.1

2.4.3 2015 Test Sections

The 2015 Test Track research cycle featured a cracking group experiment meant to examine the top-down cracking of different surface mixtures. The total AC design thickness of each section was 7 inches comprised of three asphalt lifts. The bottom two lifts were the same between all the sections and featured HiMA-with 7.0% SBS polymer modified binder to help prevent bottom-up cracking. One section (N1-Control) had 20% reclaimed asphalt pavement (RAP) in the surface mix with an unmodified binder and served as the control. In contrast, another section (S6-HiMA) was a repeat of the control section, but with 7.0% SBS polymer modified binder HiMA in the surface lift. These two sections form the basis for another comparison in this investigation. Both were trafficked for two test cycles accumulating approximately 20 MESALs from October 15, 2015 through February, 2021.

Figure 2.5 shows the as-built pavement cross sections for the 2015 sections, again noting that the same materials were used between the two sections, except for the surface lift in each section. Table 2.5 lists the as-built asphalt properties for each layer in each section. The differences in as-built properties between the sections' base and intermediate mixes were deemed insignificant for experimental purposes and within the allowance for normal pavement construction. More details regarding these sections have been previously documented [11].

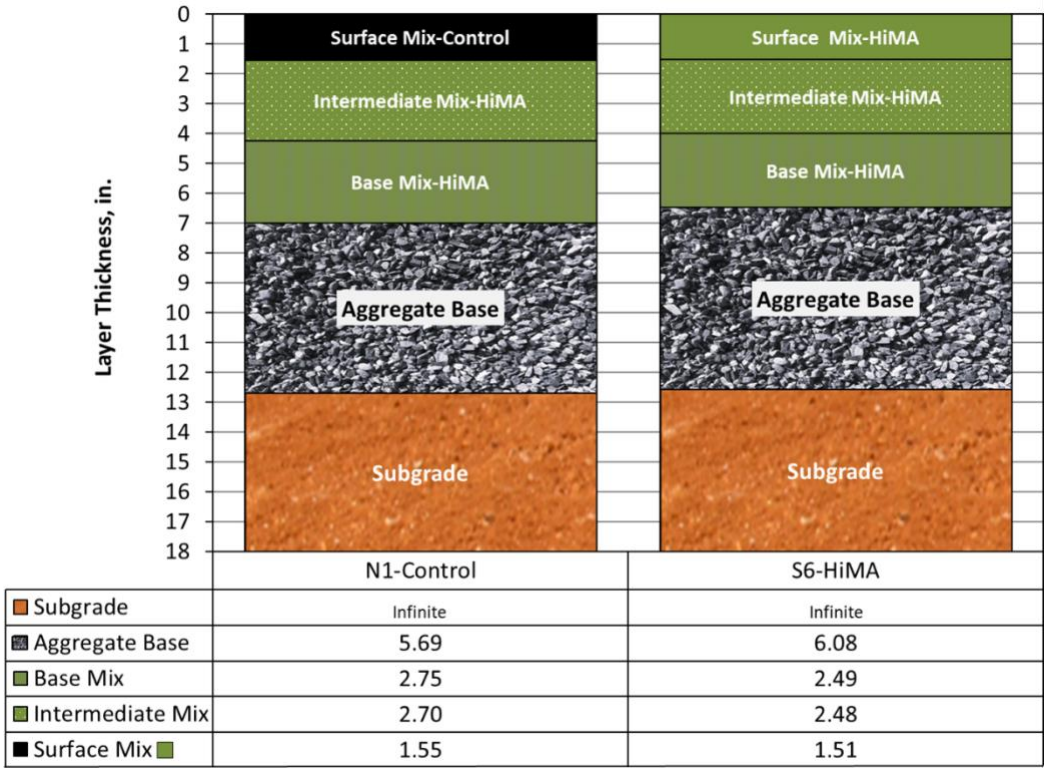

	N1-Control	S6-HiMA
Subgrade	Infinite	Infinite
Aggregate Base	5.69	6.08
Base Mix	2.75	2.49
Intermediate Mix	2.70	2.48
Surface Mix	1.55	1.51

Figure 2.5 2015 Test Sections.

Table 2.5 2015 Test Sections As-Built Asphalt Properties

Lift	Surface		Intermediate		Base	
Section	N1-Control	S6-HiMA	N1-Control	S6-HiMA	N1-Control	S6-HiMA

NMAS, mm	12.5	9.5	19.0	19.0	19.0	19.0
SBS, %	0.0	7.0	7.0	7.0	7.0	7.0
PG Grade	67-22	94-22	94-22	94-22	94-22	94-22
Asphalt Content, %	5.4	5.8	4.5	4.7	4.6	4.6
Air Voids, %	6.4	8.2	6.2	6.8	6.3	7.3
Plant Temp, °F	320	340	320	320	320	330

2.5 STRUCTURAL & PERFORMANCE CHARACTERIZATION

Each pavement section described above was subjected to accelerated trafficking over the time periods stated above during which time the sections were monitored weekly for the progression of rutting, development of cracking, and change in ride quality. These measurements were made with an ARAN van following standard test protocols. More details regarding these measurements were documented previously [11]. In addition to surface performance monitoring, routine falling weight deflectometer (FWD) testing was conducted several times per month while the sections were under traffic, from which in situ layer moduli were backcalculated. The sections were also instrumented with asphalt strain gauges at the bottom of the lowest AC layer to measure in situ tensile strain levels under trafficking. Details regarding these measurements have been previously documented [5, 6]. These data sets were used in this investigation to make structural layer coefficient computations.

In addition to field-measured performance and structural characterization, the base mixes from the 2009 test cycle (Figure 2.3, Tables 2.2, 2.3) were subjected to bending beam fatigue testing (BBFT) following AASHTO T 321-07 from which fatigue transfer functions were developed [6]. As described below, these transfer functions were used in conjunction with the in-situ strain measurements to compute structural layer coefficients for each section.

2.6 STRUCTURAL LAYER COEFFICIENT METHODOLOGIES

This investigation made use of four different methodologies to compute structural layer coefficients. The following subsections describe, in general terms, each approach, while the following section (Results and Discussion) will provide the pertinent data sets and results of the computations. Note that not every approach was used for each section since some sections did not have the requisite data to make the computation.

2.6.1 Effective Structural Number

The 1993 AASHTO Design Guide [*1*] contains a process to compute an in-situ effective structural number (SN_{eff}) using FWD test data from which a structural layer coefficient may be found. Timm et al. [3] detailed this process in the context of Test Track data sets, which was followed in this investigation as described below.

The first step was to assemble the raw FWD data with the center and outermost (72 inch offset) deflections normalized to a reference loading of 9,000 lb, as required by the 1993 AASHTO [*1*] procedure. FWD testing at the Test Track consists of replicate drops at multiple drop heights, including a target loading of 9,000 lb, though exactly 9,000 lb is not often achieved. Therefore, a simple linear interpolation approach was used to determine the deflections at 9,000 lb based on the available data, as demonstrated by the example in Figure 2.6. The figure shows the raw center (D1) and outermost (D9) measured deflection as a function of

load level. Linear trendlines were added to each series from which the deflection at 9,000 lb was computed. In this case, D1 at 9,000 lb. was computed to be 24.732 milli-in, and D9 at 9,000 lb. was computed to be 1.480 milli-in. This process was repeated for every set of FWD drops at every location in each section on each day of testing.

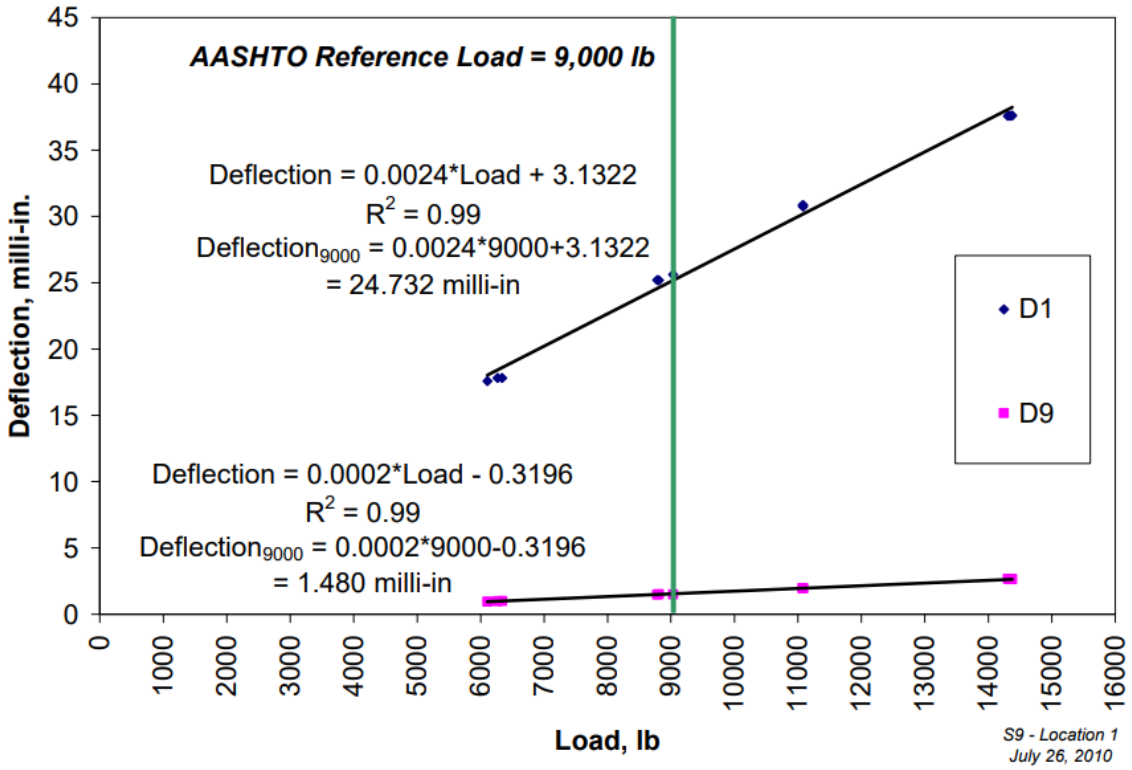

Figure 2.6 Deflection versus Load Example [12].

The second step of the process was to normalize the deflections at 9,000 lb to a reference temperature of 68°F, as required by the 1993 AASHTO procedure [1]. While the 1993 AASHTO procedure [*1*] has generic charts for normalizing deflections to this reference temperature, a more robust approach (and that taken for this study) is to develop section-specific normalized deflections. Figure 2.7 shows this process on an example data set, not affiliated with this study, with D1 and D9 deflections normalized to 9,000 lb using the process described above. The clear influence of AC temperature on D1 is evident. At the same time, D9 is much less sensitive to changes in temperature, which is expected since it represents properties of the soil that are not nearly as affected by temperature. The exponential regression equation ($y = k_1 e^{k_2 * T}$) fitted between D1 deflections at 9,000 lb and mid-depth AC temperatures (shown in Figure 2.7) was used to normalize the D1 data to a reference temperature of 68°F as follows:

$$D_{1@68} = D_{1@T} * e^{k_2 * (68 - T)} \qquad \text{(Equation 2.1)}$$

Where:

$D_{1@68}$ = Center deflection normalized to 68°F, milli-in (D1 at 68°F in Figure 2.6)
$D_{1@T}$ = Center deflection at measured temperature, T, milli-in (D1 in Figure 2.6)
T = measured mid-depth AC temperature, °F
k_2 = section-specific regression coefficient

Figure 2.7 clearly shows that temperature has been removed as a factor by the D1 at 68°F series. Also, since temperature does not significantly impact D9, no temperature correction was needed, nor was it recommended by the 1993 AASHTO procedure [*1*]. The outcome of this step was deflection data for each section that were normalized to both a reference load of 9,000 lb and a reference temperature of 68°F.

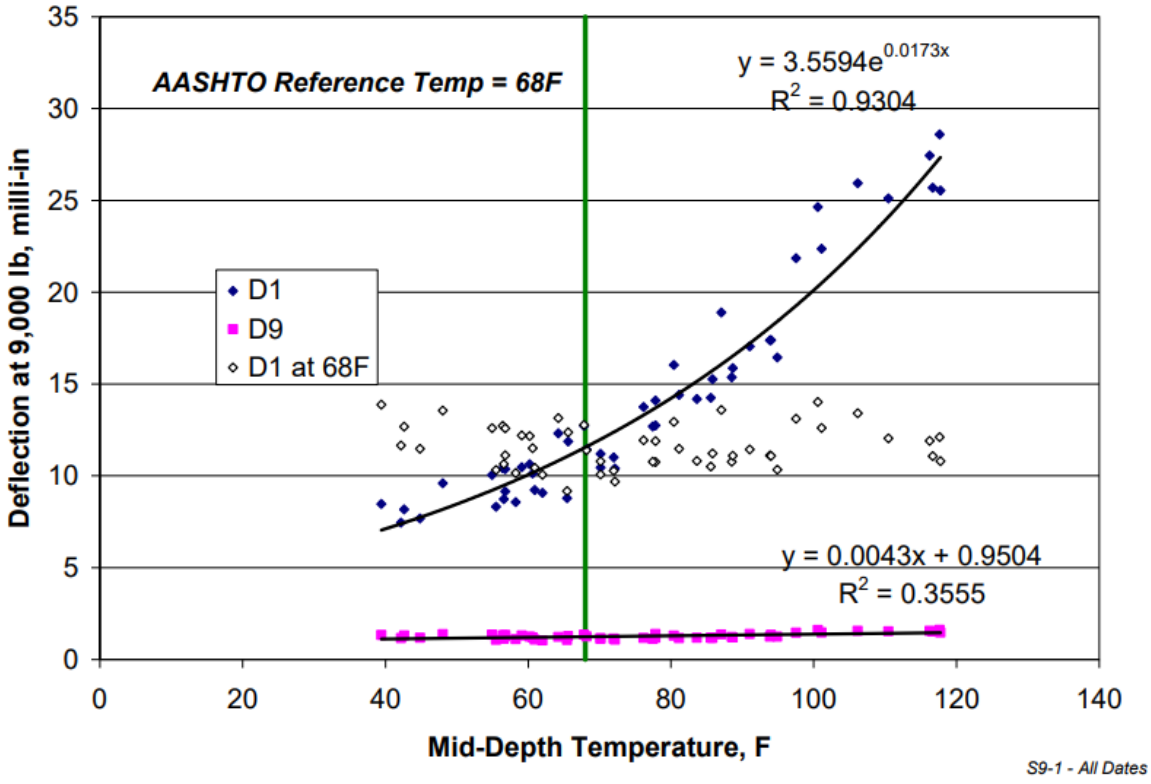

Figure 2.7 Deflection versus Temperature Example [12].

The third step in the process was to compute the soil modulus (M_R) and the composite pavement modulus (E_p) for each test location on each testing date. The M_R computation is relatively straightforward as follows [1]:

$$M_R = \frac{0.24*P}{\delta_r * r} \qquad \text{(Equation 2.2)}$$

where:

M_R = subgrade modulus, psi
P = load magnitude, lb (9,000 lb recommended by AASHTO)
δ_r = measured deflection at offset, r, normalized to 9,000 lb, in.
r = radial offset, 72 in.

Once M_R is determined for a given location on a given date, E_p may be computed by iteratively solving Equation 2.3 by bisection for E_p [1]:

$$\delta_1 = 1.5 * p * a \left(\frac{1}{M_R \sqrt{1 + \left(\frac{D}{a} \sqrt[3]{\frac{E_p}{M_R}} \right)^2}} + \frac{\left(1 - \frac{1}{\sqrt{1 + \left(\frac{D}{a} \right)^2}} \right)}{E_p} \right)$$

(Equation 2.3)

where:
δ_1 = center deflection at 68°F normalized to 9,000 lb, in. (called D1 at 68°F above)
p = contact pressure, psi (computed from load, P, and circular contact radius, a)
a = FWD load plate radius, 5.91 in.
D = total pavement depth above subgrade, in.
M_R = subgrade modulus computed from Equation 2.2, psi
E_p = composite pavement modulus, psi

Once E_p was calculated, the fourth step was to compute SN_{eff} from E_p according to the following equation:

$$SN_{eff} = 0.0045 * D * \sqrt[3]{E_p}$$

(Equation 2.4)

where:
SN_{eff} = effective structural number of in-place pavement
D = total pavement depth above subgrade, in.
E_p = composite pavement modulus, psi

Figure 2.8 shows how SN_{eff} represents the whole pavement section, including both the asphalt and granular base layers, which may be expressed as:

$SN_{eff} = a_1 * D_1 + a_2 * m_2 * D_2$ (Equation 2.5)

where:
a_1 = asphalt concrete structural layer coefficient
D_1 = asphalt concrete thickness, in.
a_2 = granular base structural layer coefficient
m_2 = granular base drainage coefficient
D_2 = granular base thickness, in.

To compute an asphalt structural layer coefficient in this approach, the underlying base structural layer coefficient must be known or assumed. In this study, as will be shown later, the granular base modulus was found to be very low, which would actually result in a negative structural layer coefficient following 1993 AASHTO correlations [*1*]. The abnormally low granular base moduli at the Test Track have been verified and well-documented in previous investigations [9]. To be conservative, a value of 0 was assigned to the granular base structural layer coefficient, and Equation 2.5 was solved for a_1 as follows:

$a_1 = SN_{eff} / D_1$ (Equation 2.6)

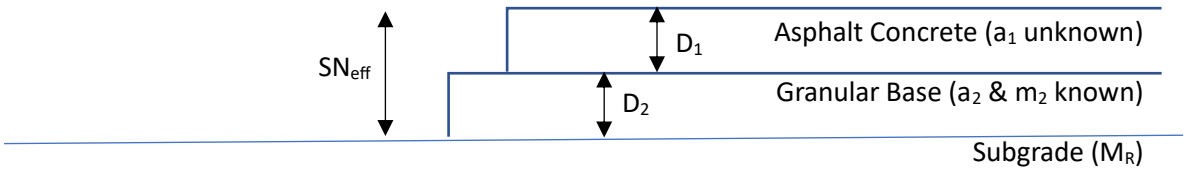

Figure 2.8 SN_{eff} Schematic.

2.6.2 Modulus Correlation

The 1993 AASHTO Design Guide [*1*] has correlations to translate layer moduli into structural layer coefficients. Figure 2.9 shows the correlation between the asphalt concrete modulus (E_{AC}) at 68°F and the asphalt layer coefficient (a_1). Notably, the chart only goes up to 500,000 psi for $E_{AC,}$ so extrapolation is needed to reach layer moduli commonly found in modern mixes used in southern climates.

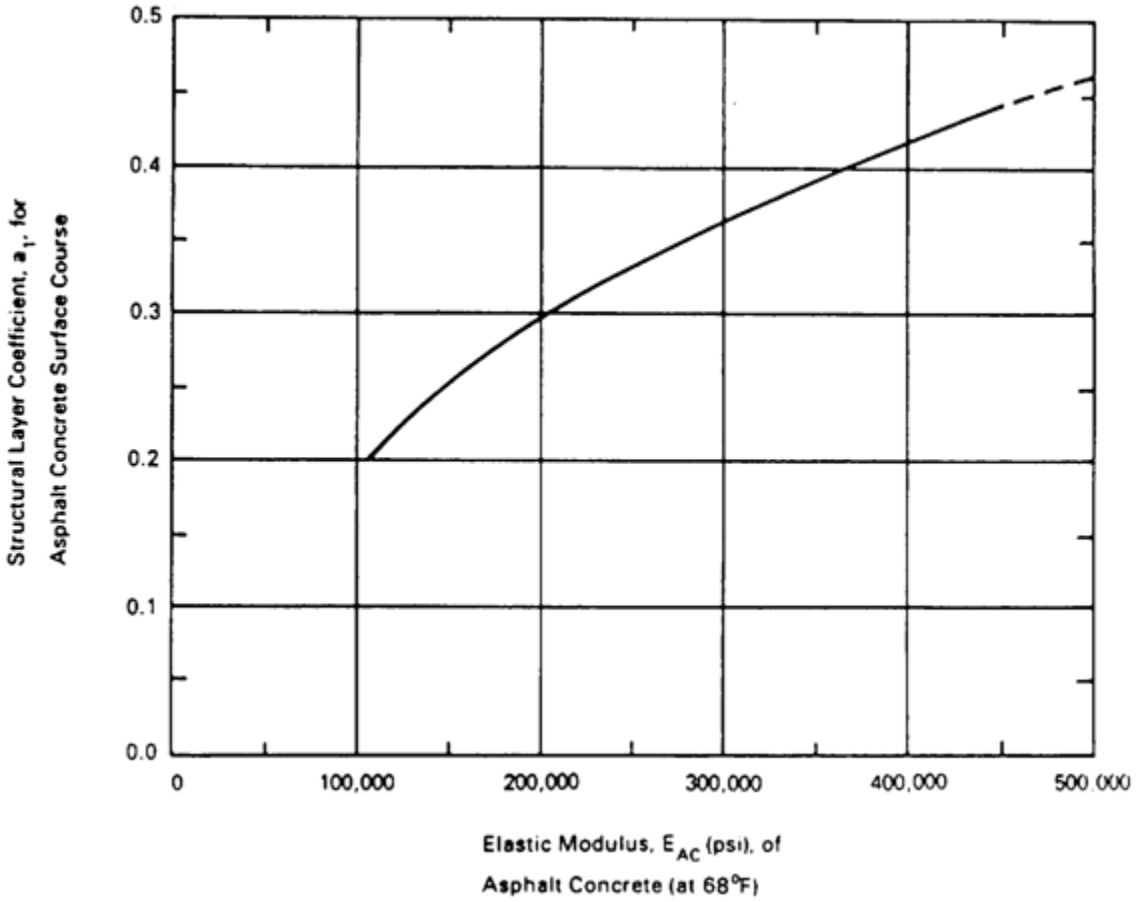

Figure 2.9 1993 AASHTO Design Guide Asphalt Structural Layer Coefficient Correlation [*1*].

The curve in Figure 2.9 was used to manually extract data points and fit a trendline in Excel, as shown in Figure 2.10. The solid black line is the best-fit natural log trendline with the corresponding equation inserted in the plot and also shown below as Equation 2.7. The dotted line shows the trendline extrapolated to the 2003 Test Track modulus value of 811,114 psi, which yields a structural layer coefficient of 0.54. It is notable that this is the exact value obtained from another approach that calibrated the structural layer coefficient based on the performance data of the same 2003 Test Track sections [4].

$$a_1 = 0.171 * ln(E_{AC@68}) - 1.784 \quad \text{(Equation 2.7)}$$

where:
a_1 = asphalt concrete structural layer coefficient
$E_{AC@68}$ = asphalt concrete modulus at 68°F, psi

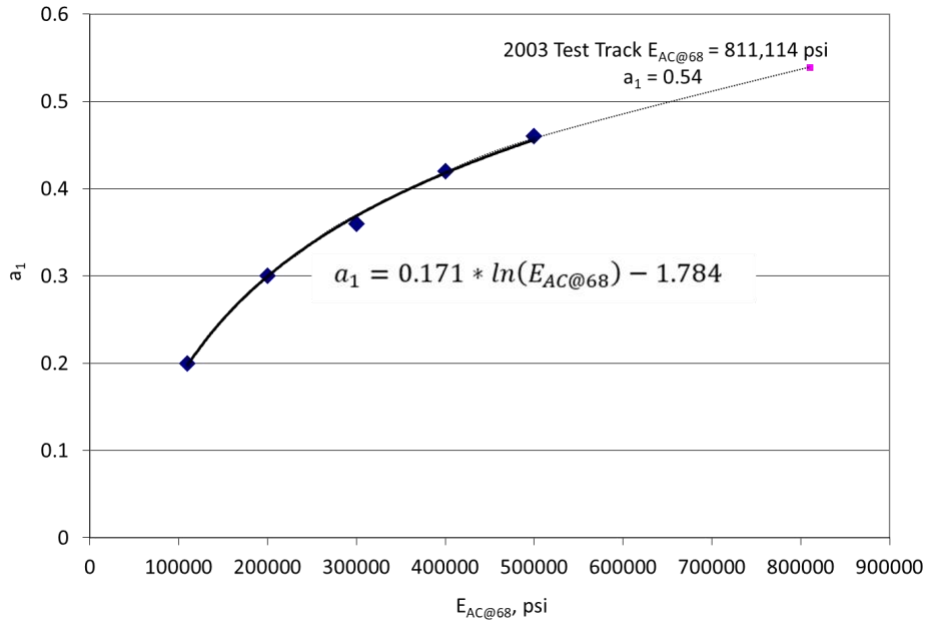

Figure 2.10 1993 AASHTO Design Guide [*1*] Asphalt Structural Layer Coefficient Correlation Extrapolation.

Estimation of asphalt concrete structural layer coefficient using Equation 2.7 relied on in situ moduli determined through backcalculation of FWD data. The same raw deflection data described above in Section 2.6.1 were used in a more comprehensive multilayer backcalculation scheme with EVERCALC 5.0 to determine in situ moduli. The backcalculation scheme determined three layer moduli (i.e., asphalt concrete, granular base, and subgrade) for a given set of deflection basin data from a single drop. Though testing was conducted at various load levels, only loadings ranging between 8,000 and 10,000 lb were used to be very close to the AASHTO target of 9,000 lb. Furthermore, a temperature correction was applied to the backcalculated AC moduli, following a similar procedure to that described for temperature correcting raw deflection data (refer to Figure 2.7) to produce AC moduli at 68°F by using the following equation:

$$E_{AC@68} = E_{AC@T} * e^{k_2*(68-T)} \quad \text{(Equation 2.8)}$$

where:

$E_{AC@68}$ = backcalculated AC modulus at 68°F, psi
$E_{AC@T}$ = backcalculated AC modulus at measured temperature mid-depth AC (T), psi
T = measured mid-depth AC temperature, °F
k_2 = section-specific regression coefficient

These corrections were done on a section-specific basis (i.e., section-specific k_2 values) to better represent the actual behavior of the section rather than rely on a generic temperature correction process. Once the moduli were corrected to the 68°F reference temperature, they were entered into Equation 2.7, from which structural layer coefficients were computed and analyzed.

2.6.3 Equivalent Sections

The equivalent section approach relied on embedded strain gauge (at the bottom of the lowest AC layer) measurements and laboratory-determined fatigue transfer functions of control, and HiMA mixes to find structurally equivalent pavement sections. The control section was used as the baseline case, and an equivalent HiMA section (thickness) was computed that would produce the same fatigue performance/life, as explained below.

The first step in this process was to determine the estimated number of cycles to fatigue cracking failure of the control section ($N_{f\text{-}control}$) based on in situ strain measurements and laboratory-determined transfer function. In situ strain measurements were collected over many months at varying temperatures and were normalized to 68°F following the same procedure described above for the raw deflection data (Equation 2.1) and backcalculated AC modulus (Equation 2.8). The average strain at 68°F ($\varepsilon_{68\text{-}control}$) was then entered into the fatigue transfer function for the control asphalt concrete determined through bending beam fatigue testing in the lab following AASHTO T321-07 to find $N_{f\text{-}control}$. More details regarding this testing were previously documented by Timm et al. [6].

Once $N_{f\text{-}control}$ was found, the transfer function for the HiMA section was used to determine the HiMA strain level ($\varepsilon_{68\text{-}HiMA}$) that would produce the same number of cycles to fatigue cracking failure of the HiMA section (i.e., $N_{f\text{-}control} = N_{f\text{-}HiMA}$). After finding $\varepsilon_{68\text{-}HiMA}$, it was necessary to compute the HiMA thickness (H_{HiMA}) that would produce this strain level. This was done by starting with the measured as-built thickness of the HiMA section ($H_{HiMA\text{-}m}$) and the measured strain level in the section at 68°F ($\varepsilon_{68\text{-}HiMA\text{-}m}$). The subscript "m" is used for both of these parameters to indicate measured values.

It is well known that there is an inverse-squared relationship between strain and AC thickness in asphalt pavements having the following functional form:

$$\varepsilon = a * H^{-2} \qquad \text{(Equation 2.9)}$$

Where:

ε = tensile strain at the bottom of the asphalt concrete layer
H = depth of asphalt concrete
a = section-specific constant

Following the format of Equation 2.9 and using the strain levels and thicknesses defined above, the following ratio can be established:

$$\frac{\varepsilon_{68-HiMA-m}}{\varepsilon_{68-HiMA}} = \frac{a*H_{HiMA-m}^{-2}}{a*H_{HiMA}^{-2}} \quad \text{(Equation 2.10)}$$

In this equation, everything is known except for the section-specific constant (a) and equivalent HiMA thickness (H_{HiMA}), but the "a" terms cancel, which allows for direct computation of H_{HiMA} as follows:

$$H_{HiMA} = H_{HiMA-m}\sqrt{\frac{\varepsilon_{68-HiMA-m}}{\varepsilon_{68-HiMA}}} \quad \text{(Equation 2.11)}$$

which is the thickness of HiMA that will yield an equivalent number of cycles to failure as the control section. The next step, after H_{HiMA} is computed from Equation 2.11, is to determine the control section's structural number. This is done by simply multiplying the measured in situ thickness ($H_{control\text{-}m}$) by a known structural layer coefficient ($a_{1\text{-}control}$):

$$SN_{control} = H_{control-m} * a_{1-control} \quad \text{(Equation 2.12)}$$

As described above, the theoretical thickness of the HiMA section (H_{HiMA}) was computed to provide structural equivalence to the control section, so the following is true:

$$SN_{control} = H_{control-m} * a_{1-control} = SN_{HiMA} = H_{HiMA} * a_{1-HiMA} \quad \text{(Equation 2.13)}$$

which can be solved for $a_{1\text{-}HiMA}$:

$$a_{1-HiMA} = \frac{H_{control-m}*a_{1-control}}{H_{HiMA}} \quad \text{(Equation 2.14)}$$

The approach described above, though somewhat complicated, has the advantage of accounting for differences in expected performance between the control and HiMA materials, whereas the previous two approaches (effective structural number and modulus correlation) only rely on the stiffness of the materials being evaluated.

2.6.4 Performance Data

The last approach, as described by Timm et al. [3], most closely follows the calibration of structural layer coefficients conducted during the AASHO Road Test [2]. This approach adjusts the asphalt structural layer coefficient to minimize the error between predicted and actual ESAL applications for a measured decrease in performance characterized by a change in serviceability.

Figure 2.11 summarizes the approach, which was previously documented [4]. As described by Timm et al. [3], "the procedure relies on two primary data sets. The first is historical traffic data in terms of axle weights, axle configuration, and volume, which are needed to compute ESALs over time. The second is performance data expressed as the International Roughness Index (IRI), which can be converted to pavement serviceability index (PSI) over time. As shown in Figure 2.11 and explained further below, these two primary data sets are used in several equations to generate the actual ESALs applied to the pavement and the predicted ESALs that the pavement is expected to withstand. Since the AC structural layer coefficient (a_1) is used to determine the structural number (SN), which appears in both the actual and

predicted ESAL equations, $\hat{a}_1$ may be iteratively adjusted to minimize the error between actual and predicted ESALs. The $\hat{a}_1$ symbol is used to indicate that it is a value that will be determined through a best-fit iterative procedure." Further details regarding this process are provided below.

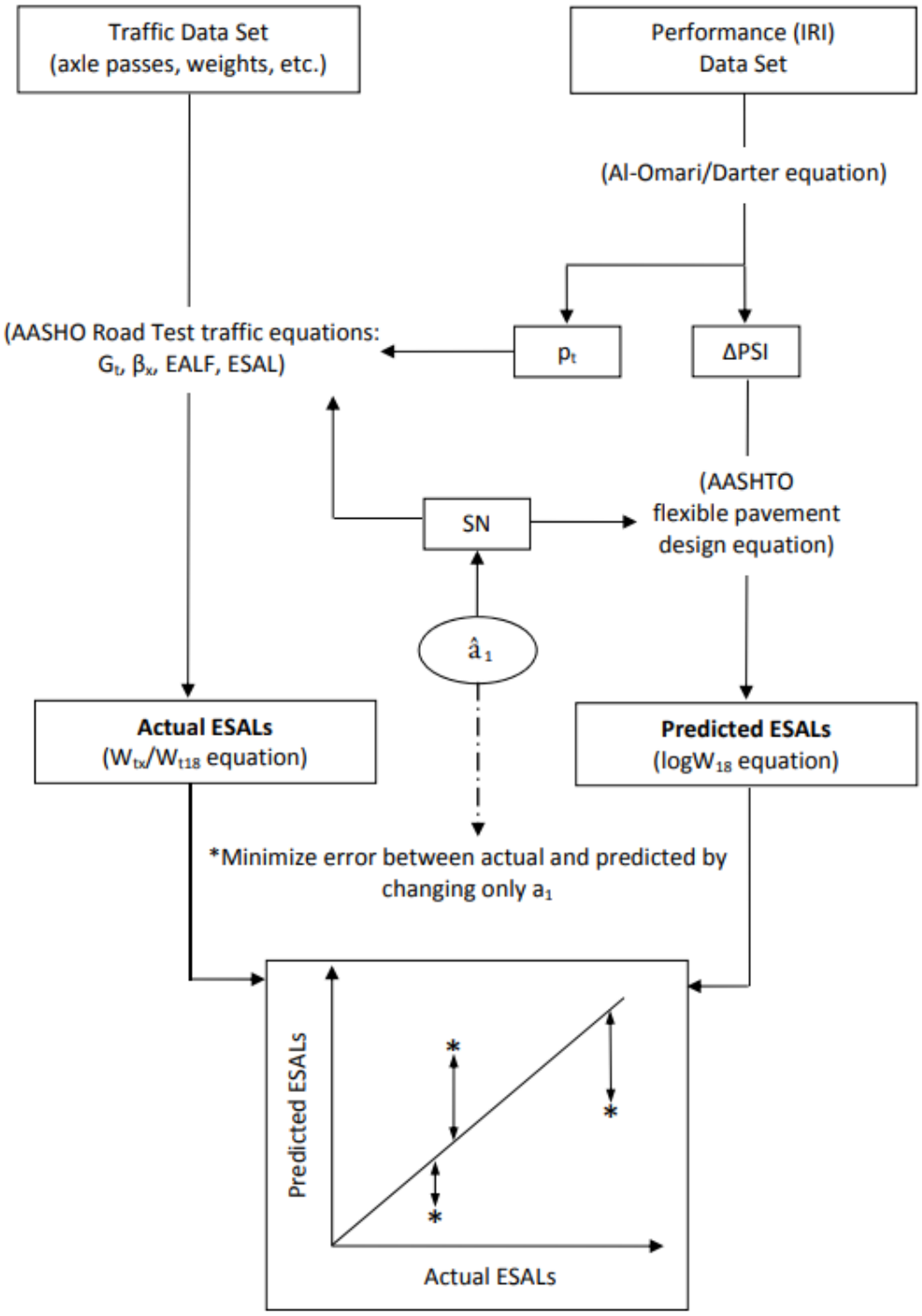

Figure 2.11 Performance-Based Calibration Procedure [4].

As noted in Figure 2.11, three equations pertain to this process. They are the Al-Omari/Darter equation, the AASHO Road Test traffic equations, and the AASHTO Flexible Pavement Design equation. The Al-Omari/Darter equation links pavement roughness to pavement serviceability as follows [13]:

$$PSI = 5e^{(-0.0038 \cdot IRI)} \quad \text{(Equation 2.15)}$$

where:
PSI = Present serviceability index (0-5 scale)
IRI = International Roughness Index, in./mile

Using Equation 2.15, the initial serviceability (p_o) may be computed from the initial IRI before trafficking, along with terminal serviceability at any point in time (p_t) computed from the IRI corresponding to a known amount of trafficking. Note that p_t, when used in AASHTO pavement thickness design, refers to the lowest acceptable or "terminal" serviceability for the design. However, when used in calibration, as was done for this investigation, it refers to a fixed point in time representing a particular serviceability corresponding to a known amount of ESAL application. The difference in these values is referred to as the change in serviceability ($\Delta PSI = p_o - p_t$), which is used directly in the AASHTO Flexible Pavement Design equation, while the p_t value is used in the AASHO Road Test Traffic equations.

The AASHO Road Test Traffic equations, shown as Equations 2.16a-d, account for the pavement's structural number, axle group type, axle group loading, and terminal serviceability to compute equivalent axle load factors (EALFs), which expresses the number of non-standard axles to equal the same amount of damage as one pass of an 18,000 lb single axle with dual tires. These computations are made on a per-axle group basis for each vehicle and then added together to determine the total number of ESALs per truck pass, also known as a truck damage factor.

$$log\left[\frac{W_{tx}}{W_{t18}}\right] = 6.1252 - 4.79\, log(L_x + L_2) + 4.33\, log\, L_2 + \frac{G_t}{\beta_x} - \frac{G_t}{\beta_{18}} \quad \text{(Equation 2.16a)}$$

$$G_t = \log\left[\frac{4.2 - p_t}{4.2 - 1.5}\right] \quad \text{(Equation 2.16b)}$$

$$\beta_x = 0.40 + \frac{0.081 \cdot \left(L_x + L_2\right)^{3.23}}{\left(SN + 1\right)^{5.19} \cdot L_2^{\,3.23}} \quad \text{(Equation 2.16c)}$$

$$EALF = 10^{log\left[\frac{W_{tx}}{W_{t18}}\right]} \quad \text{(Equation 2.16d)}$$

where:
L_x = axle group load in kips
L_2 = axle code (1 for single, 2 for tandem, and 3 for tridem)
SN = structural number
W_{tx} = number of x axle load applications at time t
W_{t18} = number of 18 kip axle load applications at time t
β_x = a function of design and load variables
β_{18} = value of β_x when L_x is equal to 18, and L_2 is equal to one
p_t = terminal serviceability determined from IRI data converted to PSI
G_t = a function of serviceability levels

At the Test Track, the trucks have the traffic parameters listed in Table 2.6, which are used with Equations 2.16a-d, along with the computed structural number using as-built thicknesses and assumed structural layer coefficients, to find the EALFs and subsequently the truck damage factor using Equation 2.17.

Table 2.6 Test Track Axle Group Loadings

Axle Group Type	Steer	Tandem	Single
Number per Truck (n)	1	1	5
Axle Code (L_2)	1	2	1
Average Group Weight, kips (L_x)	12	40	20

$$Truck\ Damage\ Factor = \sum_{i=1}^{m} EALF_i n_i \qquad \text{(Equation 2.17)}$$

where:
Truck Damage Factor = ESALs/truck
m = number of axle load groups per truck
$EALF_i$ = EALF for the i^{th} axle load group
n_i = number of axle groups having the same L_2 and L_x characteristics

Once the truck damage factor has been determined, the total ESALs to any given point in time are found by multiplying the total number of truck passes by the truck damage factor. In this study, and according to Figure 2.11, that value is referred to as the "Actual ESALs".

The computation of the "Predicted ESALs" comes from the AASHTO Flexible Pavement Design equation. As described above, a primary input to the equation is the pavement performance characterized by ΔPSI obtained through the IRI data set as shown in Equation 2.18:

$$\log W_{18} = Z_R S_0 + 9.36 \log(SN+1) - 0.20 + \frac{\log\left[\frac{\Delta PSI}{4.2-1.5}\right]}{0.4 + \frac{1094}{(SN+1)^{5.19}}} + 2.32 \log M_R - 8.07 \qquad \text{(Equation 2.18)}$$

where:
$\log W_{18}$ = predicted log ESALs
Z_R = standard normal deviate for a given reliability
S_0 = standard deviation
ΔPSI = difference between initial (p_o) and terminal (p_t) serviceability at time *t*
M_R = resilient modulus of the subgrade, psi
SN = sum of structural layer coefficient and as-built thickness products for each pavement layer

As described previously [*3*], "Equation 2.18 is normally used for design, where ESALs (W18) are input, SN is computed and a reliability in excess of 50% is used to act as a safety factor when determining the required structural number. However, in the case of recalibration, the objective is to closely match predicted and actual ESALs applied without this design safety factor applied. Therefore, reliability should be set at 50% (average), which yields a standard normal deviate equal to 0, and the $Z_R S_0$ term drops out of Equation 2.18."

It is important to emphasize the structural number (SN) link between equations 2.16a-d and 2.18. Since they both require SN input for their respective computations and because SN uses the asphalt structural layer coefficient, the structural layer coefficient can be used to minimize the error between the actual and predicted ESALs when performance and traffic data are available. A final note about this process is that it requires significant ΔPSI to work properly. If there is little to no change in IRI and consequently very small ΔPSI, equation 2.18 does not produce meaningful results. Because of this limitation, the 2009 and 2015 sections could not be calibrated by this method because they did not experience a significant change in pavement roughness. However, the 2010 section rehabilitated with HiMA and the original cross-section built in 2006 and rehabilitated in 2009 without HiMA, did have large enough changes in IRI to allow for calibration.

2.7 RESULTS AND DISCUSSION

The following subsections present the analyses of each set of test sections evaluated for this investigation, with the last subsection synthesizing all the results.

2.7.1 2009 Test Sections

The 2009 Sections (N7-HiMA and S9-Control) were subjected to effective structural number, modulus correlation, and equivalent section analysis. Calibration using performance data was not viable since neither section experienced a significant decline in serviceability to use the performance calibration process. The results of the analyses are presented below.

2.7.1.1 2009 Test Sections – Effective Structural Number

Following the effective structural number process described in Section 2.6.1, structural layer coefficients were computed for both the N7-HiMA and S9-Control sections. The data set size varied between the two sections, with the control having 802 a_1 computations compared to the HiMA section having 421. The difference was primarily due to the frequency of testing. Due to time restrictions during the 2009 research cycle, only the control section was subjected to FWD testing three times per month. The other sections, including the HiMA section, were tested on alternating test dates.

Despite the differences in data set size, both sections had significant sample sizes and the cumulative distribution of the computed a_1 values, as shown in Figure 2.12. Both sections had very similar a_1 values, especially between the 20th and 80th percentile. The tails differed more appreciably with the HiMA section, resulting in higher values. However, for design purposes, the focus should be on the 50th percentile since the 1993 AASHTO Design Guide [*1*] has a standard deviation term in the structural design equation that addresses the design variability, which includes variability of the structural layer coefficient. Though there is a small difference observed at the 50th percentile, when rounded to two decimal places, both sections produced 0.38. It is important to note that this is lower than an often-used value of 0.44 for asphalt concrete material and even more significantly lower than the 0.54 currently used in Alabama for structural pavement design. However, this method only relies on deflection data rather than performance data in determining a_1 values. Therefore, the primary finding from this particular analysis is that there was no practical difference between the control and the HiMA asphalt concrete material a_1 values when only considering pavement deflection data using the effective structural number process.

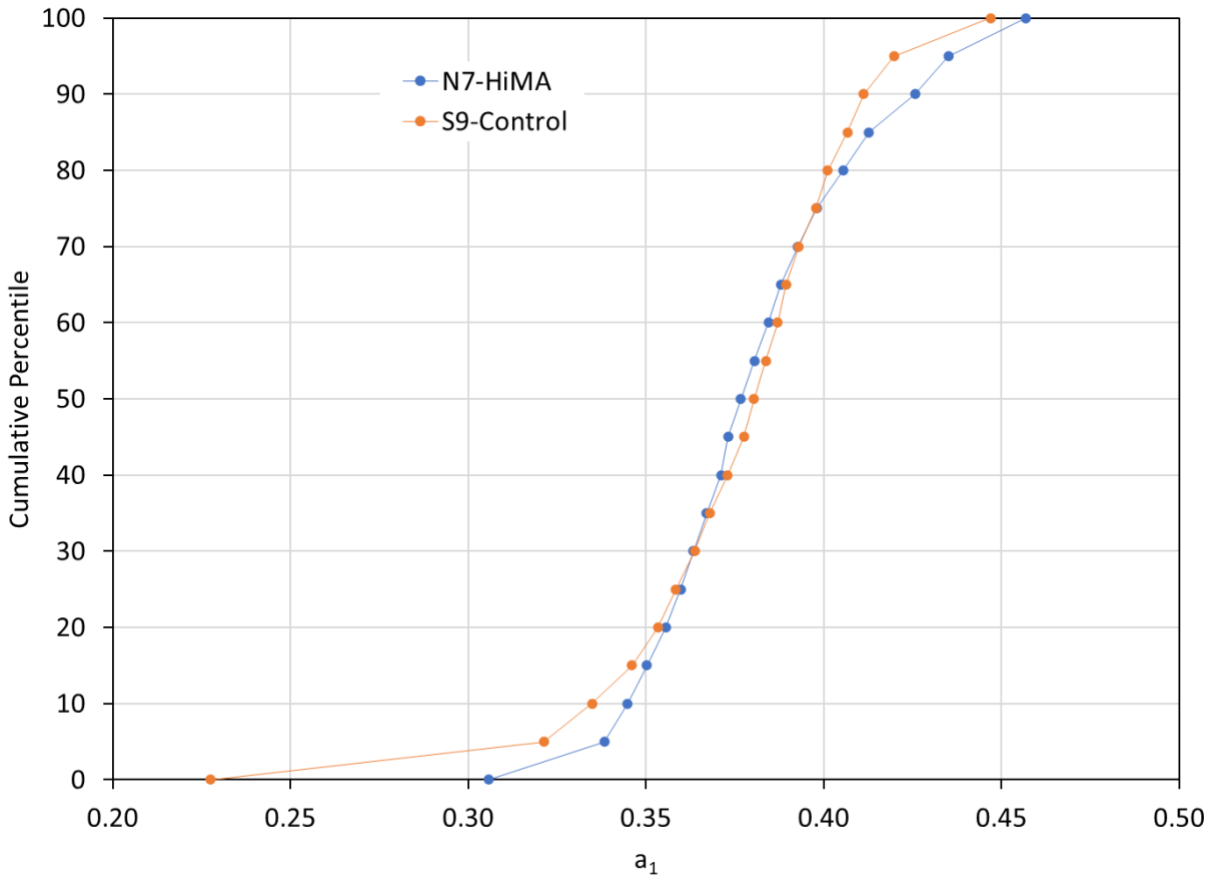

Figure 2.12 2009 Test Sections a_1 Cumulative Distributions from Effective Structural Number Analysis.

2.7.1.2 2009 Test Sections – Modulus Correlation

The cumulative distributions of a_1 determined through modulus correlation, as described in Section 2.6.2, are shown in Figure 2.13. Like the effective structural number analysis, the sample size was larger for the control section (N=2,233) compared to the HiMA section (N=1,209) due to differences in testing FWD frequency, but both sections had significant sample sizes. The computed a_1 values for both materials fell between 0.40 and 0.65, which is more in line with the value currently used in Alabama for structural pavement design (0.54). As observed in the effective structural number analysis, there was only a slight difference between the two sections at the 50th percentile. In fact, rounded to two decimal places, both sections produced a_1 values equal to 0.56. Again, like the effective structural number analysis, there was no appreciable difference between sections when only considering the backcalculated in situ modulus of the pavement without considering the respective performance characteristics. In other words, modulus alone is not enough to distinguish between the materials and may be misleading from a performance perspective.

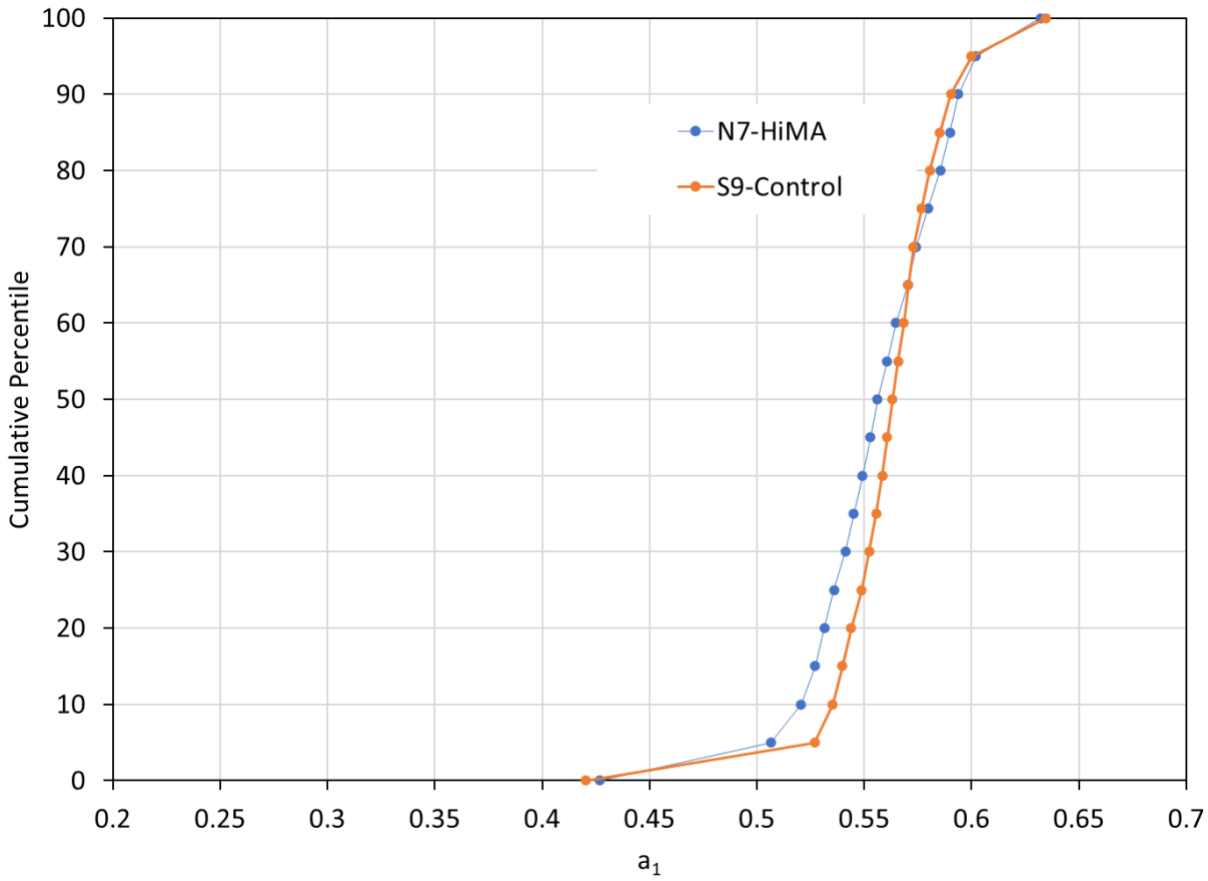

Figure 2.13 2009 Test Sections a_1 Cumulative Distributions from Modulus Correlation Analysis.

2.7.1.3 2009 Test Sections – Equivalent Sections

The equivalent section approach was used with the 2009 test sections following the procedure described in Section 2.6.3. Figure 2.14 shows the first step, where the two-year average field-measured strain of the control section normalized to 68°F ($\varepsilon_{68\text{-control}}$ = 372 με) was used with fatigue transfer function of the control to estimate the number of cycles to fatigue cracking failure of the control section ($N_{f\text{-control}}$ = 263,026). This value was then set for the number of cycles to fatigue cracking failure of the HiMA section ($N_{f\text{-control}} = N_{f\text{-HiMA}}$ = 263,026), which was used with the HiMA transfer function to find the strain level of the HiMA section ($\varepsilon_{68\text{-HiMA}}$ = 589 με) that would produce the same number of cycles to failure.

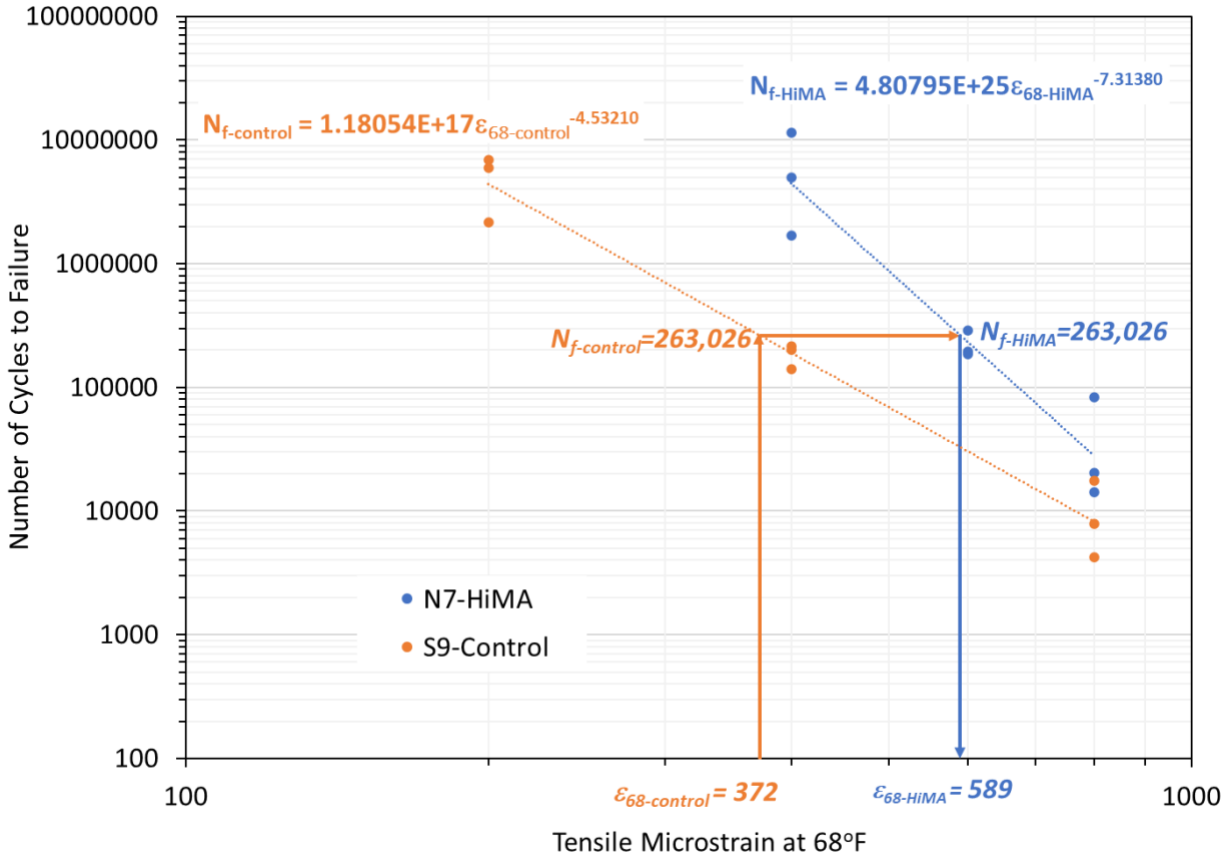

Figure 2.14 2009 Sections Equivalent Thickness Analysis – Step 1.

The next step was to find the equivalent thickness of HiMA (H_{HiMA}) from the strain level computed above ($\varepsilon_{68\text{-HiMA}}$ = 589 με), the field-measured strain level in the HiMA section at 68°F ($\varepsilon_{68\text{-HiMA-m}}$ = 345 με), and the as-built thickness of the HiMA section ($H_{HiMA\text{-m}}$) using equation 2.11 (repeated here for convenience):

$$H_{HiMA} = H_{HiMA-m}\sqrt{\frac{\varepsilon_{68-HiMA-m}}{\varepsilon_{68-HiMA}}} \qquad \text{(Equation 2.11 (repeated))}$$

While the strain levels in the equation above are fixed based on the computations explained above, the as-built thickness of the HiMA section ($H_{HiMA\text{-m}}$) could be considered in several ways to arrive at the equivalent HiMA section thickness (H_{HiMA}). The first approach uses the section-wide average as-built thickness from the twelve FWD locations that had surveyed depths determined during construction. The advantage of this approach is it considers the entire section, but the disadvantage is that strain measurements were not made across the entire section. The second approach only uses the thickness in the center of the strain gauge array. The advantage of this approach is that it ties the thickness directly to the strain measurement but doesn't consider the entire section. Since both were deemed equally valid, results from both approaches are presented below.

The final step of the process was to compute the structural layer coefficient of the HiMA section ($a_{1\text{-HiMA}}$), using the as-built thickness of the control section ($H_{control\text{-m}}$) and equivalent HiMA thickness (H_{HiMA}), after

assuming a structural layer coefficient of the control section ($a_{1\text{-control}}$) using Equation 2.14 (repeated here for convenience):

$$a_{1-HiMA} = \frac{H_{control-m} * a_{1-control}}{H_{HiMA}} \quad \text{(Equation 2.14 (repeated))}$$

As described above, the HiMA thickness to arrive at the same number of cycles to fatigue failure as the control was computed in two ways, which meant the control section was also represented in two ways (i.e., section-wide or gauge array). A further issue was in selecting the $a_{1\text{-control}}$ value. For this analysis, the $a_{1\text{-control}}$ was set at 0.44 (commonly used by many state DOTs) and 0.54 (used by the Alabama DOT).

The 2x2 factorial resulting from two different thicknesses and two different control structural layer coefficients resulted in four computed HiMA structural layer coefficients, as shown in the bottom row of Table 2.7. As expected, the lowest values were computed when $a_{1\text{-control}}$ was 0.44 since they had a relatively lower starting point. Also, the values were higher for the gauge array condition compared to the section-wide condition since the difference in the as-built AC thickness between the control and HiMA sections was greater in that location than the section-wide average. Since the section-wide and gauge array conditions were considered equally valid, it makes sense to average the values together for a given control structural layer coefficient. This yields the following values:

- a_{1HiMA} = 0.75 ($a_{1control}$ = 0.44)
- a_{1HiMA} = 0.92 ($a_{1control}$ = 0.54)

Table 2.7 2009 HiMA Structural Layer Coefficients Computed from Equivalent Thicknesses

	Scenario			
Property	Section-Wide $a_{1\text{-control}}$ = 0.44	Section-Wide $a_{1\text{-control}}$ = 0.54	Gauge Array $a_{1\text{-control}}$ = 0.44	Gauge Array $a_{1\text{-control}}$ = 0.54
HiMA As-Built Thickness, in. ($H_{HiMA\text{-}m}$)	5.64		5.04	
HiMA Equivalent Thickness, in. (H_{HiMA})	4.32		3.86	
Control as-built Thickness, in. ($H_{control\text{-}m}$)	7.00		6.83	
HiMA Structural Layer Coefficient ($a_{1\text{-}HiMA}$)	0.71	0.88	0.78	0.96

2.7.1.4 2009 Test Sections – Summary

The 2009 sections (N7-HiMA and S9-Control) were subjected to effective structural number, modulus correlation, and equivalent thickness methods of computing HiMA material structural layer coefficients. The first two approaches, which essentially only relied on in-place properties, produced no differences in structural layer coefficients between the control and HiMA asphalt concrete material. However, the third method, which took into account both the field-measured strain levels and laboratory-determined fatigue transfer functions, found that N7-HiMA could have been built significantly thinner to achieve the same expected fatigue cracking performance. This resulted in the following recommended structural layer coefficients, depending on the assumed control structural layer coefficient, which were computed by averaging the values in Table 2.7 for a particular assumed control structural layer coefficient:

- a_{1HiMA} = 0.75 ($a_{1control}$ = 0.44)
- a_{1HiMA} = 0.92 ($a_{1control}$ = 0.54)

2.7.2 2010 Test Section

The section rehabilitated with HiMA in 2010 was somewhat complicated since the section was originally built in 2006, milled and inlayed with the same materials in 2009 before having the HiMA mill and inlay in 2010. Therefore, a step-wise calibration was done, following the performance data calibration procedure described in Section 2.6.4, to make the HiMA discernable from the underlying distressed pavement, as detailed below. Also, since this section spanned several test cycles and had significant cracking, it was decided not to use the other three methods of calibration since the data may have been unreliable.

2.7.2.1 2010 Test Section - Stepwise Performance Data Calibration

The steps listed below were used in the calibration process of the 2010 HiMA section and are shown schematically in Figure 2.15. It should also be noted that the subgrade modulus, determined through backcalculation, was used in Equation 2.18. This value was 12,155 psi, which also took into account the 0.33 correction factor recommended by the 1993 AASHTO Design Guide [*1*].

- Step 1 – Find a_1 for the original asphalt concrete placed in 2006.
- Step 2 – Assign the a_1 from Step 1 to the new but same material placed in 2009 and find the structural layer coefficient of the distressed pavement left in place ($a_{cracked}$).
- Step 3 – Assign $a_{cracked}$ from Step 2 to the left in place asphalt and find the structural layer coefficient of the HiMA layer (a_{HiMA}).

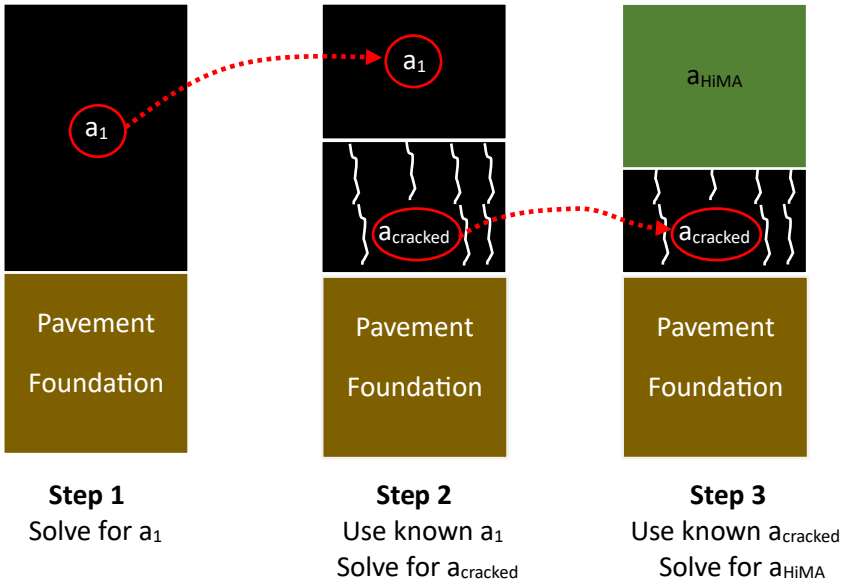

Figure 2.15 2010 Stepwise Performance Data Calibration.

The predicted versus measured ESALs for Step 1 are shown in Figure 2.16, resulting from the best fit a_1 of 0.39 for the original asphalt concrete placed in 2006 It should be noted that only ΔPSI values exceeding 0.5 were used since anything less produced nonsensical data, which means data at lower ESAL values are not represented. However, ESALs in the higher range (above 5 million) closely follow the line of equality with a nearly 1:1 slope on the trendline with a high R^2 value of 0.98, which indicates a good match between measured and predicted ESALs (i.e., it was a good calibration). Also, the data do not fully reach 10 MESALs that is commonly used to describe a full trafficking cycle at the Test Track. This is because 10 MESALs corresponds to the number of truck passes multiplied by a generic truck damage factor (12.8 ESALs/truck) which is used for computing ESALs for all the Test Track sections. For this investigation, truck damage factors were computed using Equation 2.16 for each section based on the SN resulting from the calibrated structural coefficient. These section specific values were then multiplied by the number of truck passes for a more accurate representation of ESALs. In this case, it did not reach 10 MESALs.

Figure 2.17 shows the predicted versus measured ESALs for Step 2, where the assumed a_1 was 0.39, based on the result from Step 1, and the computed $a_{cracked}$ was 0.2. Note that 0.2 is in the AASHTO-recommended range for medium to high-severity alligator cracking [1], which is a good confirmation of the calibration process. Like Step 1, only ΔPSI values exceeding 0.5 were used, which limited the amount of data for calibration but yielded a very strong match between measured and predicted ESALs at the end of the service life before the next rehabilitation was done with HiMA.

Figure 2.18 shows the predicted versus measured ESALs for Step 3, where the $a_{cracked}$ used was 0.20, based on Step 2, and the computed a_{HiMA} was 0.92 to produce a reasonable match between measured and predicted ESALs with admittedly more scatter in the data than Steps 1 and 2. Interestingly, this value was the same as that generated from investigating the 2009 sections when assuming 0.54 for the control material in the equivalent sections methodology. It is also important to note that the calibration made use of ΔPSI values exceeding 0.2, in contrast to Steps 1 and 2, which used 0.5 or greater. This was done because

there were no ΔPSI values exceeding 0.5 since the section performed so well. The maximum ΔPSI was 0.36.

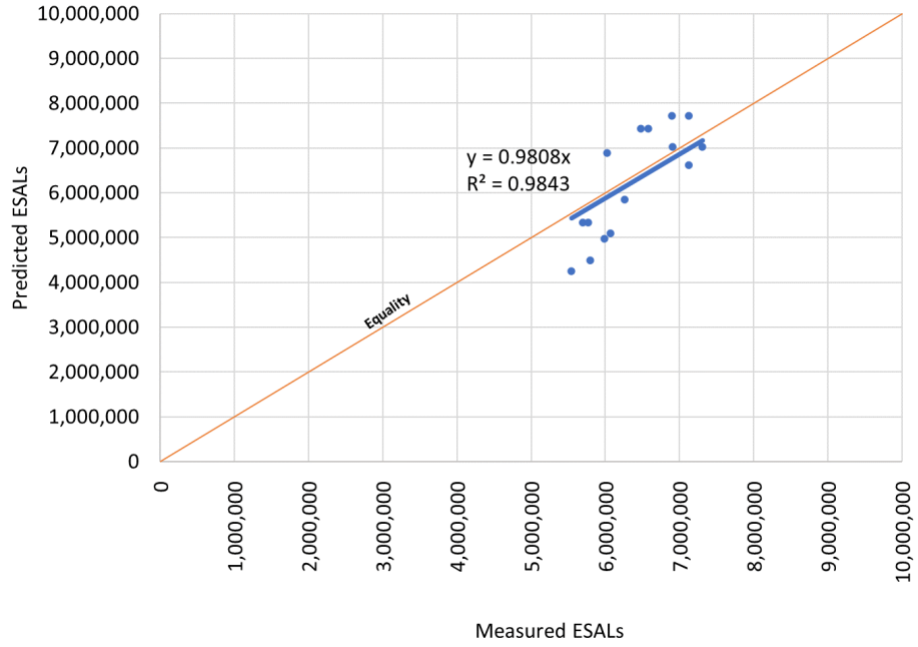

Figure 2.16 – 2010 Performance Data Calibration Step 1 (computed a_1 = 0.39).

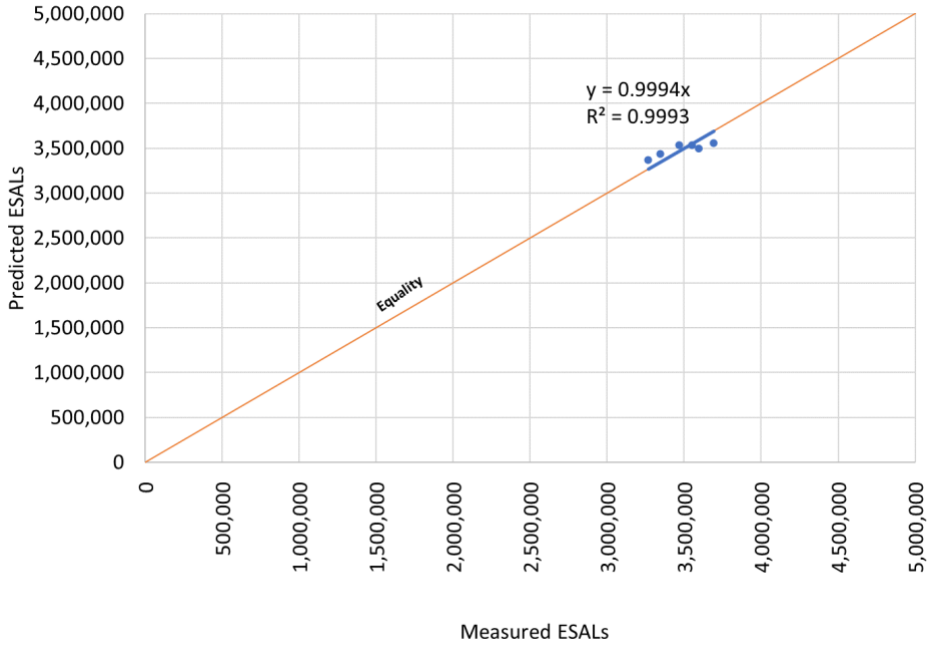

Figure 2.17 2010 Performance Data Calibration Step 2 (assumed a_1 = 0.39; computed $a_{cracked}$ = 0.2).

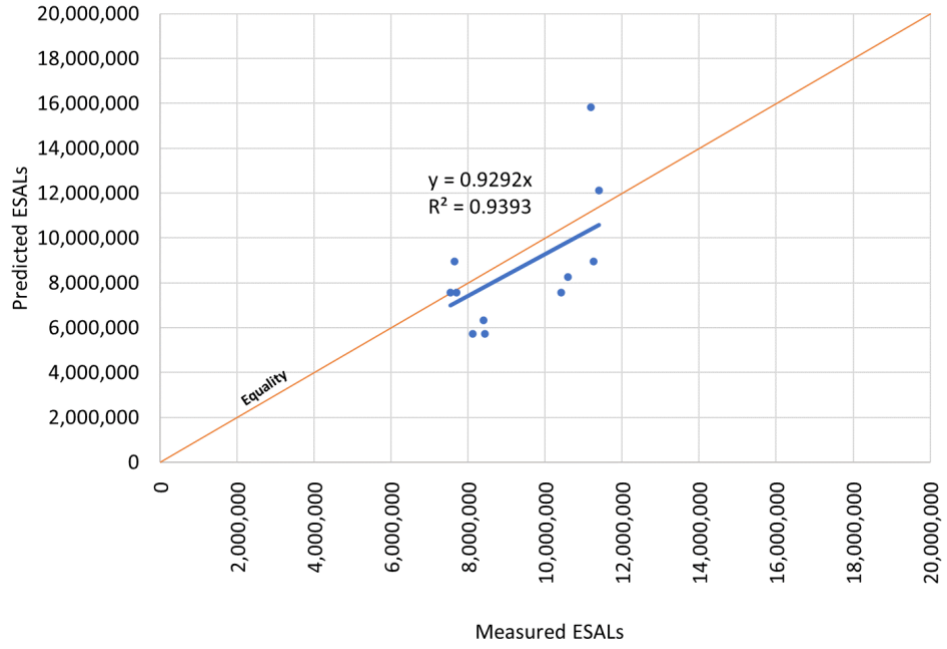

Figure 2.18 2010 Performance Data Calibration Step 3 (computed a_{HiMA} = 0.92; assumed $a_{cracked}$ = 0.2).

2.7.3 2015 Test Sections

Recall that the 2015 sections (S6-HiMA and N1-Control) were built as part of a common experiment with the same design thicknesses, though the as-built thicknesses varied slightly. The sections had the same HiMA mixtures in the base and binder courses (binder modified with SBS 7% polymer), but the N1-Control surface course did not contain polymer modified binder, while section S6-HiMA had HiMA with 7% SBS polymer modified binder. The sections were subjected to effective structural number and modulus correlation analysis, as described in the following subsections. Calibration using performance data was not an option since these sections did not experience a significant change in IRI. Also, these sections did not have enough working strain gauges to provide the needed data for the equivalent section analysis.

2.7.3.1 2015 Test Sections – Effective Structural Number

Like the 2009 test sections, these sections were analyzed according to the effective structural number approach described in Section 2.6.1. The sample size for S6-HiMA was 844, while the N1-Control sample size was 835. These sample sizes were more similar in this test cycle because the sections received the same frequency of FWD testing over the two-year period.

Figure 2.19 shows the cumulative distribution of structural coefficients for each section, denoted by S6-HiMA and N1-Control, respectively. Though there is a spread to the data, it is relatively narrow, covering a range between 0.45 and 0.75, with the 50th percentile values shown next to the respective series. S6-HiMA produced a 50th percentile value of 0.65, which was 0.05 greater than that of N1-Control. This slight difference was attributed to the surface layer in S6-HiMA, which was HiMA with 7% SBS polymer modified binder, while the control section was unmodified.

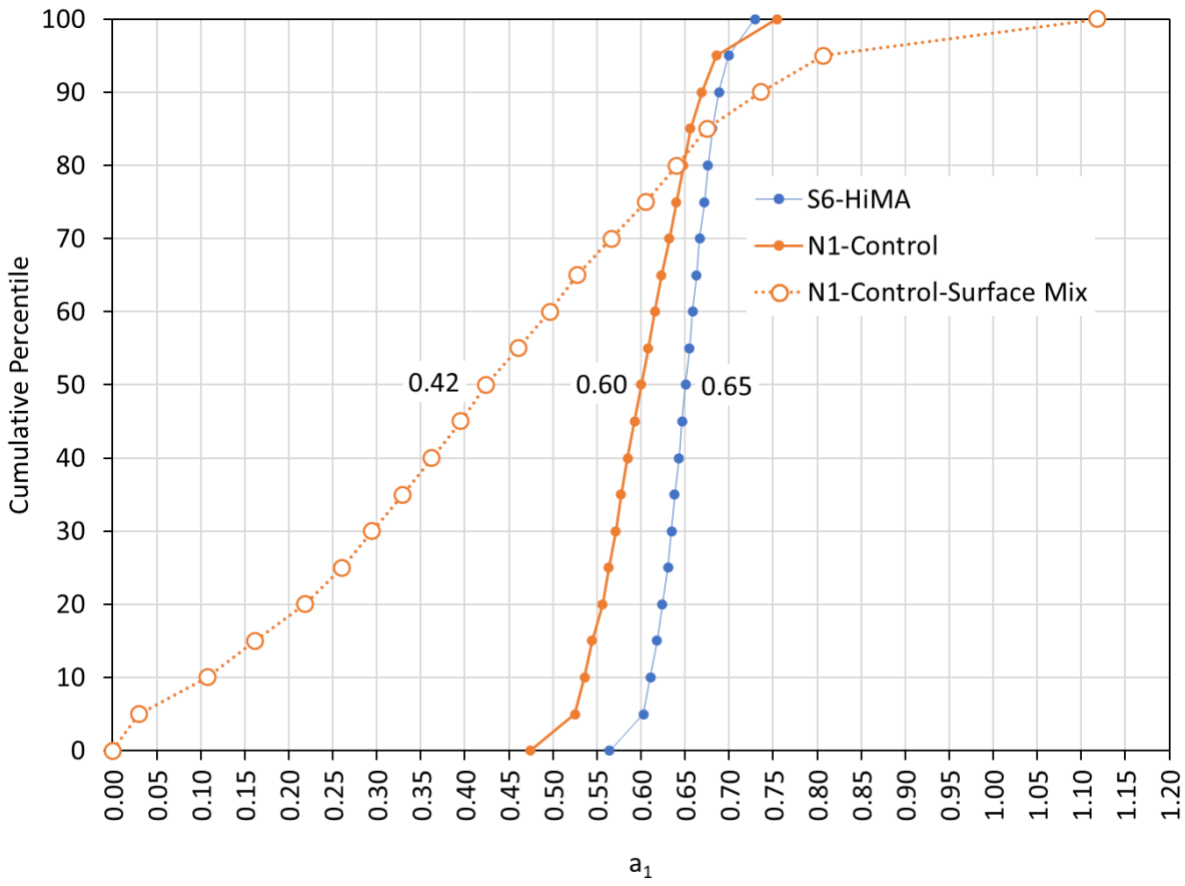

Figure 2.19 2015 Test Sections a_1 Cumulative Distributions from Effective Structural Number Analysis.

Since N1-Control contained both polymer-modified (HiMA) and un-modified lifts, an additional computation was made to separate the non-HiMA lifts from the HiMA lift. Figure 2.20 shows schematically how this was done. First, the 50th percentile structural layer coefficient of 0.65 from Figure 2.19 for S6-HiMA was assigned to all the layers in S6 and the two bottom layers (base and binder courses) in N1-Control. Next, with a known structural layer coefficient value of 0.65 for the bottom layers in N1-control, along with knowing the as-built thicknesses of the HiMA layers (D_{HiMA}) and control surface layer ($D_{control}$) in N1-control, and having an SN_{eff} computed from the FWD data, the structural layer coefficient of the surface lift in N1 ($a_{1\text{-}control}$) was computed with the equation shown in Figure 2.20. Essentially, the structural layer coefficient was found by subtracting the structural contribution of the HiMA lifts in N1-control from the computed effective structural number and dividing by the thickness of the surface lift. This resulted in a distribution of values, shown in Figure 2.19 as the "N1-Control-Surface Mix" series. Interestingly, the 50th percentile value of the surface mix was 0.42 according to this methodology, which is very close to an often used value for asphalt materials of 0.44. Also, it is important to point out that it is computationally possible to achieve zero or negative values for $a_{1control}$ using the equation in Figure 2.20 since D_{HiMA} and a_{HiMA} were computed separately from SN_{eff} in the control section. Any time the product of D_{HiMA} and a_{HiMA} exceeded the SN_{eff} from the control section, $a_{control}$ would necessarily become negative. In these cases a value of 0.0 was assigned to $a_{1control}$ that happened in less than 5% of the overall computations.

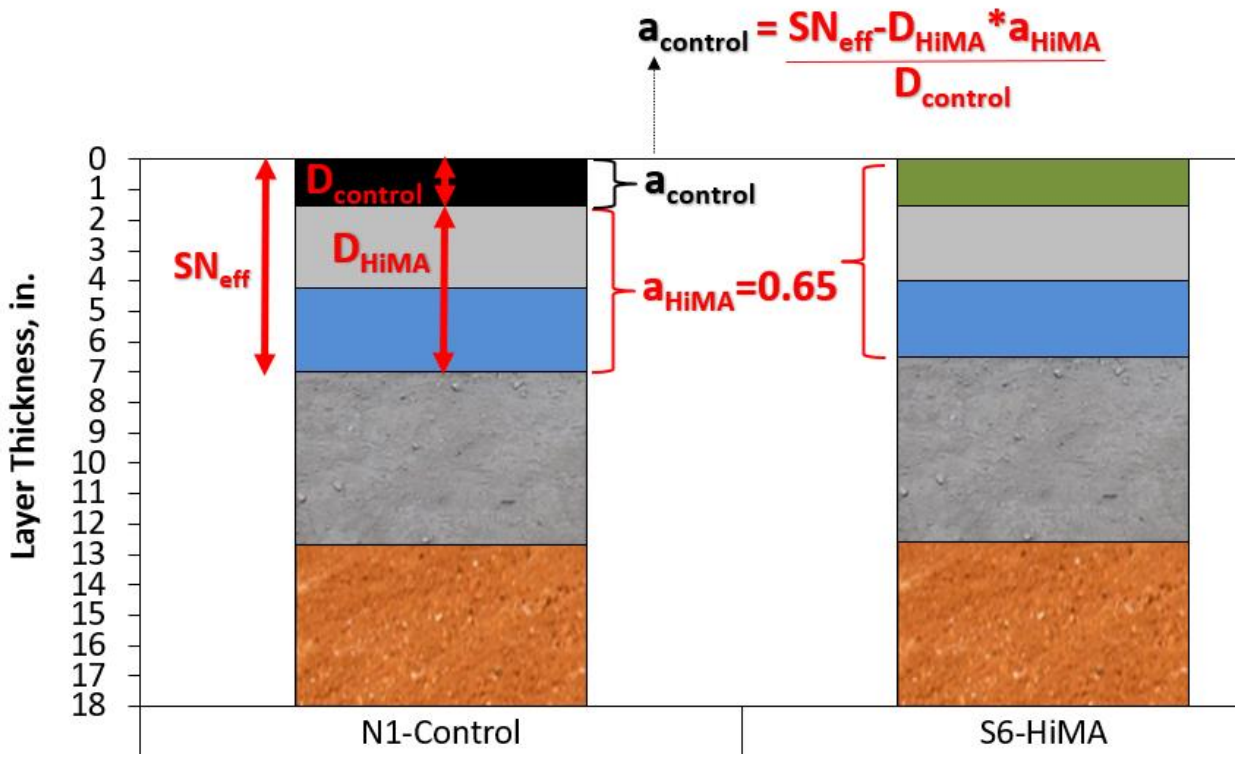

Figure 2.20 Computing $a_{1control}$ of the Surface Mix in 2015 N1-Control.

2.7.3.2 2015 Test Sections – Modulus Correlation

The results of the modulus correlation investigation of the 2015 sections are presented in Figure 2.21. The sample sizes were 1,528 and 1,439 for S6-HiMA and N1-Control, respectively. Unlike the effective structural number analysis conducted on these sections, the resulting 50th percentile structural layer coefficients were very similar, with only a 0.02 difference between them. This was deemed a practically insignificant difference, and the two were judged equally in this analysis.

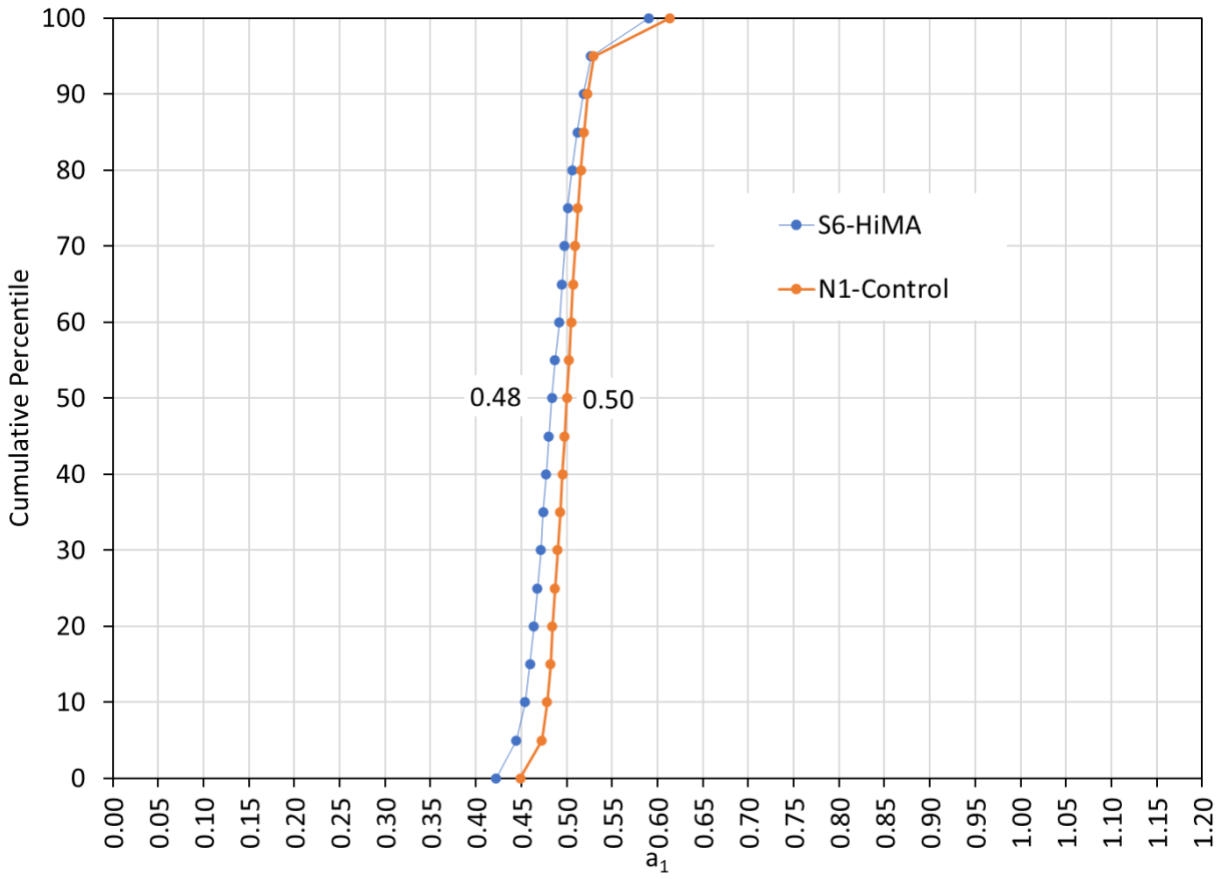

Figure 2.21 2015 Test Sections a_1 Cumulative Distributions from Modulus Correlation Analysis.

2.7.3.3 2015 Test Sections – Summary

The 2015 Sections (S6-HiMA and N1-Control) were subjected to the effective structural number and modulus correlation methods of computing structural layer coefficients. The first approach yielded a HiMA structural layer coefficient equaling 0.65, with the control surface lift on N1-Control having a value of 0.42. The modulus correlation analysis did not find a practically significant difference between the sections.

SUMMARY, CONCLUSIONS & RECOMMENDATIONS

The objective of this investigation was to compute and recommend an asphalt concrete structural layer coefficient for high-modulus asphalt mixtures (HiMA) to be used in the 1993 AASHTO Design Guide [*1*] for flexible pavements. Data from three different sets of test sections at the NCAT Test Track were used, in conjunction with four different computational methodologies, to determine a range of structural layer coefficients. Based on the data presented in this chapter, the following conclusions and recommendations are made:

1. Methods that relied only on computing structural layer coefficients from in situ material properties determined through FWD testing and backcalculation (i.e., SN_{eff} and Modulus Correlation) did not distinguish the HiMA sections from the control sections. This was expected since these methods essentially assume the same performance characteristics for a given asphalt concrete modulus.
2. The Equivalent Sections approach, used with the 2009 sections, took into account both the in situ strain measurements and laboratory fatigue performance data distinguished between the HiMA and control AC materials. Values from 0.71 to 0.96 for HiMA were computed, depending on how the data were grouped and what was assumed for the control structural layer coefficient (0.44 or 0.54). Recommended values from these sections were 0.75 and 0.92, corresponding to control structural layer coefficients of 0.44 and 0.54, respectively.
3. Calibrating to performance data, which was only possible with the 2010 rehabilitation section, resulted in 0.92 for the HiMA structural layer coefficient, which was identical to the 0.92 found from the Equivalent Sections approach with the 2009 sections when 0.54 was assumed for the control material.
4. Since the two approaches that considered performance both resulted in 0.92, it is recommended to use a_{HiMA} = 0.92 when 0.54 would be assigned to conventional materials (i.e., either unmodified or modified at typical polymer contents). To be conservative, it is recommended to use a_{HiMA} = 0.75 if conventional materials would have 0.44 for their structural layer coefficient.

CHAPTER 3: LIFE CYCLE ASSESSMENT OF HIMA PAVEMENT SECTION

3.1 INTRODUCTION

The increase in traffic, coupled with climate change, is having a significant impact on asphalt pavements, affecting their durability and service lives. Therefore, there is an increasing interest in HiMA binders as a potential solution to enhance the performance of asphalt mixtures and pavements. HiMA mixtures contain asphalt binders typically modified with 7 to 8 percent styrene-butadiene-styrene (SBS) polymer. In 2009, two test sections, Section N7 (HiMA section) and Section S9 (control section), were built on the NCAT test track to evaluate the performance benefits of HiMA mixtures as compared to unmodified mixtures and mixtures modified with typical polymer dosages of 2.8% SBS, shown in Figure 2.3.

Section N7 had surface, intermediate, and base AC layers containing asphalt mixtures with HiMA binder (7.5% SBS). The control section (S9) had surface and intermediate AC layers with typical (2.8% SBS) polymer-modified binders and unmodified base course. From an environmental impact perspective, the production of SBS polymer is energy-intensive and has a higher environmental impact, leading to higher emissions for producing one ton of HiMA mixture compared to conventional mixtures. However, it is important to note that the HiMA section is 1.36 inches thinner than the control section. The reduced thickness of the HiMA section could offset the higher environmental impacts from the production of the HiMA mixture. Therefore, a comparative life cycle assessment (LCA) needs to be conducted following ISO 14044 (ISO, 2006) to evaluate the environmental impacts of Sections N7 and S9 [14].

3.2 GOAL AND SCOPE

The goal of this analysis was to conduct a comparative cradle-to-grave life cycle assessment of Sections N7 and S9, which was constructed at the NCAT Test Track in 2009. To achieve this, the LCA analysis was separated into two subtasks. First, a cradle-to-constructed comparative LCA of Sections N7 and S9 was conducted with a functional unit of one test section, 200 ft. in length and 12 ft. in width. Then, the system boundary was extended to cradle-to-grave to include future maintenance and rehabilitation activities. Table 3.1 presents the system boundary for the cradle-to-grave LCA, per ISO 14044 (2006). For the cradle-to-grave LCA, the functional unit is one lane mile, with a lane width of 12 ft. An analysis period of 35 years, as recommended by West et al. for life cycle cost analysis (LCCA) in Alabama [15], was used for the cradle-to-grave LCA. The LCA analysis was conducted using the OpenLCA tool.

Table 3.1 System Boundary Used for the Study [14].

Production Stage			Construction Stage		Use stage							End-of-life			
Raw Materials	Transport	Manufacturing	Transport	Construction	Use	Maintenance	Repair	Replacement	Refurbishment	Operational energy use	Operational water use	Demolition	Transport	Waste processing	Disposal
A1	A2	A3	A4	A5	B1	B2	B3	B4	B5	B6	B7	C1	C2	C3	C4
✓	✓	✓	✓	✓	**X**	✓	✓	✓	✓	**X**	**X**	**X**	**X**	**X**	**X**

✓*: Life cycle stage included in the LCA*

X: *Life cycle stage excluded from the LCA*

Three pavement life cycle stages were excluded from the LCA in this study, namely use (B1), operational energy use (B6), and operational water use (B7). The use phase (B1) was omitted due to the absence of a standardized methodology for measurement among the LCA community despite its significance in LCA results. Additionally, the construction of the subgrade and granular base was excluded from the LCA, as the subgrade and granular layers were the same for both test sections. Asphalt concrete pavements are typically rehabilitated by milling and filling with an asphalt overlay rather than removing the entire structure for reconstruction [16]. Therefore, the removal or demolition stages are not a common practice at the end of life [16], so this LCA does not include emissions associated with end-of-life (C1-C4) operations.

The Tool for Reduction and Assessment of Chemical and Other Environmental Impacts (TRACI 2.1) and Cumulative Energy Demand (CED) impact assessment methods were used in this study [17, 18]. The life cycle impact indicators (LCIA) quantified in this study, and their definitions are as follows.

- Acidification
- Eutrophication
- Global Warming
- Ozone depletion
- Smog formation
- Non-renewable resources (fossil).

Acidification: Measures the potential for acidifying compounds to cause harm to terrestrial and aquatic ecosystems. This indicator is important for understanding the impact of emissions like SO_2 and NO_x, which can lead to acid rain. Acidification is expressed in kilograms of SO_2 equivalents (kg SO_{2eq}).

Eutrophication: Measures the potential for nutrients to cause over-enrichment of water bodies, leading to excessive algae growth and oxygen depletion. This indicator helps assess the impact of nutrient runoff. Eutrophication is expressed in kilograms of nitrogen equivalents (kg N_{eq}).

Global Warming: Measures the potential contribution to climate change due to greenhouse gas emissions. This indicator helps assess the impact of emissions like CO_2, CH_4, and N_2O on global Warming. Global Warming is expressed in kilograms of carbon dioxide equivalents (CO_{2eq}).

Ozone depletion: Measures the potential for substances to deplete the stratospheric ozone layer. This indicator helps assess the impact of chlorofluorocarbons (CFCs) and other ozone-depleting substances. Ozone depletion is expressed in kilograms of CFC-11 equivalents (kg CFC_{11eq}).

Smog formation: Measures the potential for volatile organic compounds (VOCs) and other precursors to form smog. This indicator helps assess the impact of emissions like VOCs and NO_x on air quality and human health. Smog formation is expressed in kilograms of ozone equivalents (kg O_{3eq}).

Non-renewable resources (fossil): Measures the potential for depletion of fossil fuel resources. This indicator helps assess the sustainability of energy use and the reliance on non-renewable resources. Non-renewable resources are expressed in megajoules (MJ).

3.3 LIFE CYCLE INVENTORY

The data needed for conducting an LCA can be categorized into two types: foreground and background data. Foreground data involve direct measurement or observation of processes directly relevant to the LCA under consideration. Background data includes inventories that describe emission intensities of upstream processes within the defined system boundaries but are not directly observed or measured in the LCA [19]. This section describes the foreground and background/upstream data used for the comparative LCA in this study.

3.3.1 Foreground data

The AC mixtures used for Sections S9 and N7 were designed without recycled materials. The quantities of aggregate and asphalt binder in these mixtures were calculated for one short ton of each AC mixture based on the as-built mixture properties determined through laboratory testing during production in 2009, as shown in Table 3.2. This information was used to quantify the environmental impacts of the raw material extraction stage (A1).

Table 3.2 Material Quantities Used for Producing Asphalt Mixtures Used in Sections S9 And N7

Mixture Type	**Section S9 (Control)**			**Section N7 (HiMA)**		
Lift (1=surface; 2=intermediate, 3=base)	1	2	3	1	2	3
Binder PG Grade	76-22	76-22	67-22	88-22	88-22	88-22
Polymer Modification, %	2.8	2.8	0	7.5	7.5	7.5
Quantity of aggregate, ton/ton of mix	93.9	95.6	95.3	93.7	95.4	95.4
Quantity of asphalt binder, ton/ton of mix	6.1	4.4	4.7	6.3	4.6	4.6
Total asphalt mix quantity used for the section, tons	14.6	31.1	38.0	17.6	41.5	44.8

During the construction of Sections S9 and N7 in 2009, foreground data needed to quantify the environmental impacts of the transportation of raw materials to the asphalt plant (A2) and asphalt plant energy consumption (A3) were not collected. However, as part of the Additive Group experiment in

2021, these transportation and plant energy data were collected for the East Alabama Paving (EAP) asphalt plant, the same plant used to produce the mixtures in Sections S9 and N7 in 2009. Virgin aggregates were sourced from Wadley, AL, 46.5 miles from the EAP plant, and asphalt binder was sourced from Birmingham, which is 171 miles from the EAP plant. The EAP plant consumed an average of 235 cubic feet of natural gas as burner fuel and 2.78 kWh of electricity to produce a ton of asphalt mix. The data collected for the Additive Group experiment was used as surrogate data for mixtures produced in 2009 for Sections S9 and N7.

The EAP plant is located 5.9 miles away from the Test Track. This information was used to quantify the environmental impacts of asphalt mix hauling (A4) from the plant to the Test Track. As data for the fuel consumption of construction equipment for the construction of Sections S9 and N7 in 2009 was not available, information from the 2021 Additive Group experiment was used. Since the thickness of the Additive Group sections differed from those of Sections S9 and N7, the construction equipment diesel consumption information was normalized to the actual paving thickness. The material transfer vehicle (MTV), paver, and rollers consumed an average of 2.0, 0.6, and 1.0 gallons of diesel for paving one inch of AC layer of a test section, which is 200 ft. long and 12 ft. wide. This information was used with as-built thickness data for Sections S9 and N7 to calculate diesel consumption from construction equipment for paving different layers of Sections S9 and N7. Table 3.3 presents average diesel consumption information from the Additive Group sections for paving a Test Track section, normalized to thickness. Information from Table 3.3 was used to quantify the environmental impacts of the constriction stage (A5) of Sections S9 and N7.

Table 3.3 Construction Equipment Diesel Consumption for the Construction of Sections S9 and N7

Equipment Type	**Section S9 (Control)**			**Section N7 (HiMA)**		
Lift (1=surface; 2=intermediate, 3=base)	1	2	3	1	2	3
Material Transfer Vehicle (MTV), gallons	2.4	5.6	6.0	2.0	4.2	5.1
Paver, gallons	0.7	1.6	1.7	0.6	1.2	1.4
Rollers, gallons	1.3	2.9	3.2	1.1	2.2	2.7

3.3.2 Background data

Wildnauer et al. (2019) developed a life cycle inventory (LCI) for the production process of neat asphalt binders and SBS-modified binders with 3.5% SBS modification in North America [20]. However, the LCI for the styrene-butadiene-rubber (SBR) polymer production process was used as a proxy to represent SBS polymer production. In 2022, the Asphalt Institute conducted a cradle-to-gate LCA for SBS polymer production, which is presented in Table 3.4 [21]. The LCIs for neat binder developed by Wildnauer et al. (2019) and SBS polymers developed by AI (2022) were used to create inventories for SBS-modified binders with 2.8% and 7.5% of SBS modification used in Sections S9 and N7, as shown in Table 3.4 [20]. However, there is a data gap for the environmental impacts associated with the terminal blending of neat binder and SBS polymer.

Table 3.4 Life Cycle Inventory for SBS Polymer and Asphalt Binders Used for Sections S9 and N7 [20, 21]

Impact Indicator	Environmental Impacts per kg of material			
	SBS polymer	*Neat binder*	*2.8% SBS modified binder*	*7.5% SBS Modified binder*
Acidification, kg SO_{2eq}	3.92E-03	1.77E-03	1.83E-03	1.94E-03
Eutrophication, kg N_{eq}	3.08E-04	1.66E-04	1.70E-04	1.77E-04
Global Warming, kg CO_{2eq}	2.88	0.64	0.70	0.81
Ozone depletion, kg CFC_{11eq}	8.09E-09	2.71E-11	2.53E-10	6.32E-10
Smog formation, kg O_{3eq}	9.44E-02	3.60E-02	3.76E-02	4.04E-02
Non-renewable, fossil, MJ	8.53E+00	5.33E+01	5.20E+01	4.99E+01

The inventory created by Mukherjee (2021) for coarse aggregate production from crushed stone was used to represent the upstream emission intensity of aggregate production in this study. This inventory was developed using data published by Marceau et al. in 2007 [22, 23]. Other LCIs were sourced from the federal LCA Commons database for upstream processes such as transportation by truck, natural gas combustion, and electricity generation, as shown in Table 3.5. It should be noted that the NAPA PCR prescribes the same inventories for asphalt mixture production, except for the SBS polymer-modified binder [24]. Additionally, the life cycle inventories developed by the Environmental Protection Agency (EPA) for off-road construction equipment were used for the construction equipment operations during the construction stage [25].

Table 3.5 Life Cycle Inventory for Upstream Inventories [20-22, 24, 25]

Asphalt Mix Life cycle stage	Activity Type	Upstream inventory	Reference
A1	Aggregate	Crushed stone, sand, and gravel	Mukherjee (2021)
A1	Asphalt binder, neat	Asphalt binder, no additives, consumption mix, at terminal, from crude oil.	Wildnauer et al. (2019)
A1	SBS polymer	Styrene-butadiene-styrene block copolymer (SBS)	Asphalt Institute (2022)
A2	Transportation by truck	Transportation by combination truck, diesel powered	NREL (2024)
A3	Natural gas	Natural gas, combusted in industrial equipment	NREL (2024)
A3	Electricity	Electricity; at grid; consumption mix - Southeast - FERC	NREL (2024)
A4	Transportation, end dump truck	Transport, single unit truck, diesel powered	NREL (2024)
A5	Paver, tailpipe emissions	Operation of diesel equipment; industry average; > 56 kW and < 560 kW - US	NREL (2024)
A5	MTV, tailpipe emissions	Operation of diesel equipment; industry average; > 56 kW and < 560 kW - US	NREL (2024)
A5	Rollers, tailpipe emissions	Operation of diesel equipment; industry average; > 56 kW and < 560 kW - US	NREL (2024)

3.4 CRADLE-TO-CONSTRUCTED

3.4.1 As-Built Test Track Section LCA results

The above-described LCA methodology was followed to perform a cradle-to-constructed comparative LCA between Sections S9 and N7. First, a cradle-to-gate LCA (A1-A3) was conducted for all six mixtures used in the different layers of Sections S9 and N7, with a declared unit of one short ton, as shown in Table 3.6. The HiMA mixtures used in the surface, intermediate, and base layers of Section N7 had higher environmental impacts compared to the conventional asphalt mixtures used in Section S9. The higher environmental impacts are due to the higher emission intensity of SBS polymer production compared to the neat asphalt binder, as shown in Table 3.4.

Specifically, the global warming potential (GWP) of the HiMA mixtures was 15%, 9%, and 12% higher for the surface, intermediate, and base layers, respectively, compared to the conventional mixtures. These findings are consistent with previous studies, which reported increases in GWP for SBS polymer-modified asphalt mixtures. A study conducted by Salehi et al. (2022) in Australia reported a 10% increase in cradle-to-gate GWP for asphalt mixtures with 8% SBS polymer-modified binder compared to conventional AC mixtures [26]. Another study reported a higher increase of 22% in GWP emissions to produce HiMA mixtures with 10-14% SBS modification compared to conventional AC mixtures [27]. This higher

increase in percent reported by Lorena et al. (2024) could be due to the use of higher polymer content compared to HiMA mixtures used in this study.

Table 3.6 Cradle-to-Gate Environmental Impacts of Producing One Ton of Asphalt Mixture

Impact Indicators	Section S9 (Control)			Section N7 (HiMA)		
Lift (1=surface; 2=intermediate, 3=base)	1	2	3	1	2	3
Acidification, kg SO2 eq	1.48E-01	1.46E-01	1.42E-01	1.58E-01	1.54E-01	1.54E-01
Eutrophication, kg N eq	1.15E-02	1.14E-02	1.10E-02	1.23E-02	1.20E-02	1.20E-02
Global Warming, kg CO2 eq	55.9	54.7	51.5	63.7	60.4	60.4
Ozone depletion, kg CFC-11 eq	8.18E-08	7.83E-08	6.94E-08	1.04E-07	9.45E-08	9.45E-08
Smog formation, kg O3 eq	3.80E+00	3.76E+00	3.66E+00	4.05E+00	3.94E+00	3.94E+00
Non-renewable, fossil, MJ	2.71E+03	2.69E+03	2.65E+03	2.81E+03	2.76E+03	2.76E+03

While the cradle-to-gate LCA results provide useful environmental impact information, they should be considered in the context of the structural cross-sections of Sections S9 and N7 for comparison. Therefore, the LCA was extended to include the entire cradle-to-constructed process, incorporating the as-built cross sections of the pavement, as follows:

- As mentioned in Section 3.2, the functional unit for the comparative LCA is one Test Track section, which is 200 ft. in length and 12 ft. in width.
- The as-built thickness and density information from Figure 2.3 and Tables 2.2 and 2.3 were used to estimate the total tonnage of asphalt mixtures used for construction of each lift of Sections S9 and N7, as presented in Table 3.2.
- The mix tonnage, mix hauling distance, and construction equipment fuel usage data (Table 3.3) were used to quantify cradle-to-constructed environmental impacts of Sections S9 and N7.

Figure 3.1 presents the GWP emissions of the as-built cross sections of Sections S9 and N7 from the cradle-to-constructed system boundary. The asphalt mixture production stage (A1-A3) had a significant impact on cradle-to-constructed emissions, as the mix hauling (A4) and construction (A5) stages contributed less than 10% of the GWP emissions.

Even though HiMA mixtures had higher cradle-to-gate environmental impacts compared to conventional mixes (Table 3.6), the cradle-to-constructed GWP for Section N7 was 9% lower than that of Section S9. The reduction is attributed to the thinner section (1.36 inches thinner) of Section N7 compared to Section S9, leading to a lower tonnage of HiMA mixtures used in construction. Figure 3.2 presents the relative environmental impacts of Sections S9 and N7, showing a 3 to 17% reduction in impact indicators for Section N7.

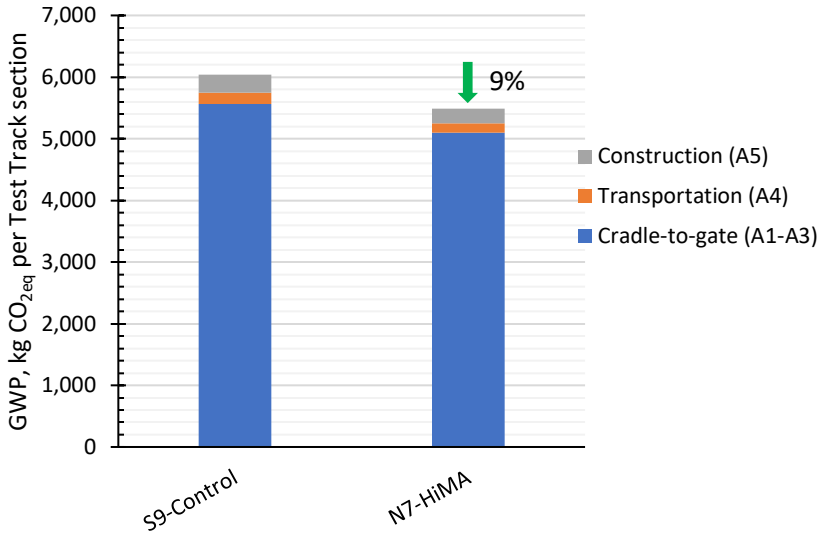

Figure 3.1 Cradle-to-Constructed Global Warming Potential of Sections S9 and N7

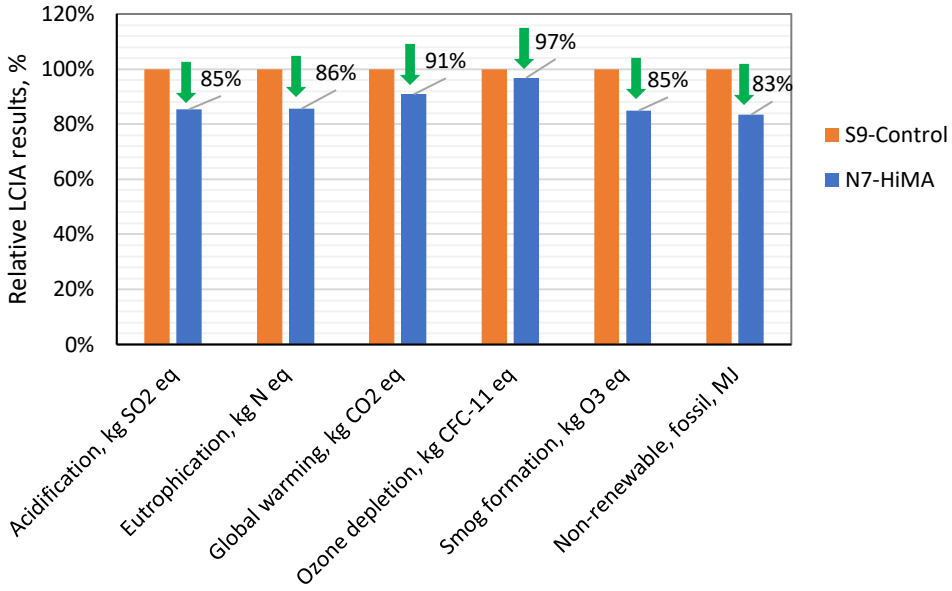

Figure 3.2 Cradle-to-Constructed Relative Environmental Impacts of Sections S9 and N7

3.4.1 Equivalent Thickness LCA results

Section 4.2.3.7 of ISO 10400 states, "*In a comparative study, the equivalence of the systems being compared shall be evaluated before interpreting the results. Consequently, the scope of the study shall be defined in such a way that the systems can be compared. Systems shall be compared using the same functional unit and equivalent methodological considerations, such as performance, system boundary, data quality, allocation procedures, decision rules on evaluating inputs and outputs, and impact assessment*" regarding a comparative LCA of two products or systems.

After 20 million ESALs of trafficking, Section N7 demonstrated better cracking and rutting field performance compared to Section S9 [11]. Therefore, a more comprehensive LCA is needed to compare the environmental impacts of the two sections due to their differing performance. To enable more reasonable LCA comparisons, an "equivalent thickness" approach was utilized in this section.

This approach involves determining the theoretical AC thickness required for Section N7 to be structurally equivalent (have the same overall structural number) to Section S9, as follows.

- The structural number for Section S9 was computed by multiplying the overall AC thickness with a layer coefficient of 0.54 (conventional mixtures), following Equation 2.12. This resulted in a structural number of 3.8 for Section S9.
- Chapter 2 of this report presented recalibrated layer coefficients for HiMA mixtures and recommended a value of 0.92 to be used for HiMA mixtures when a layer coefficient of 0.54 is used for conventional mixtures. As described above, the theoretical overall AC thickness of Section N7 (H_{HiMA}) was computed to provide structural equivalency to Section S9, following Equation 2.13, which can be solved for H_{HiMA}:

$$H_{HiMA} = \frac{H_{control} * a_{1-control}}{a_{1-HiMA}} \quad \text{(Equation 3.1)}$$

where:
H_{HiMA} = overall AC thickness of Section N7 for structural equivalency, in.
$H_{control}$ = overall as-built AC thickness of Section S9, in.
$a_{1\text{-control}}$ = layer coefficient for control/conventional mixtures, 0.54.
$a_{1\text{-HiMA}}$ = layer coefficient for HiMA mixtures, 0.92

- The theoretical overall AC thickness for Section N7 was then calculated using Equation 3.1, and the HiMA section needs 4.2 inches of AC to be structurally equivalent to Section S9 with an as-built AC thickness of 7.0 inches, as shown in Figure 3.3.

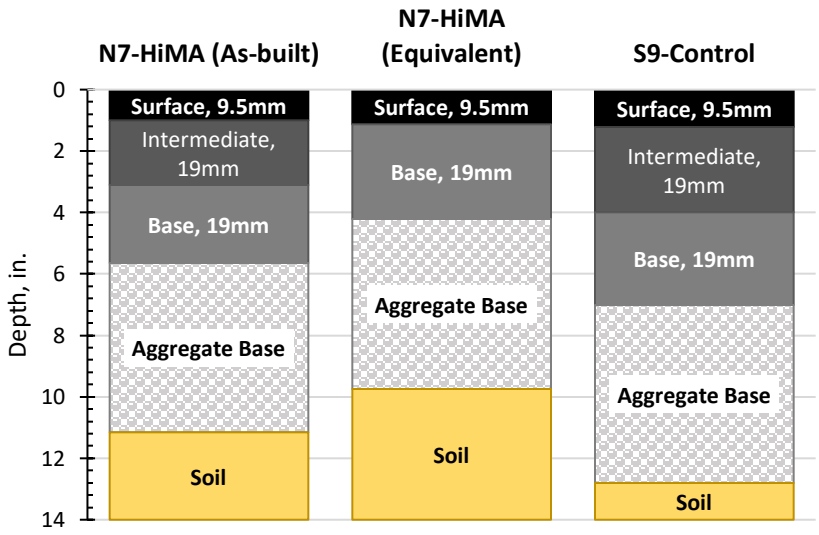

Figure 3.3 As-Built and Structurally Equivalent Cross Sections of Sections S9 and N7

The cradle-to-constructed LCA analysis was then conducted using the as-built cross-section of Section S9 and the structurally equivalent cross-section of Section N7, as shown in Figure 3.3. Figure 3.4 presents the cradle-to-constructed GWP emissions of Section S9 and structurally equivalent Section N7. The significant reduction in AC thickness of Section N7 resulted in a 31% reduction in GWP emissions compared to Section S9. This trend was also observed for other impact indicators, with reductions ranging from 24% to 37%, as presented in Figure 3.5. This analysis shows that, despite the higher cradle-to-gate environmental impacts of HiMA mixtures, the cradle-to-constructed environmental impacts of Section N7 with HiMA are lower due to its more efficient design and reduced material usage.

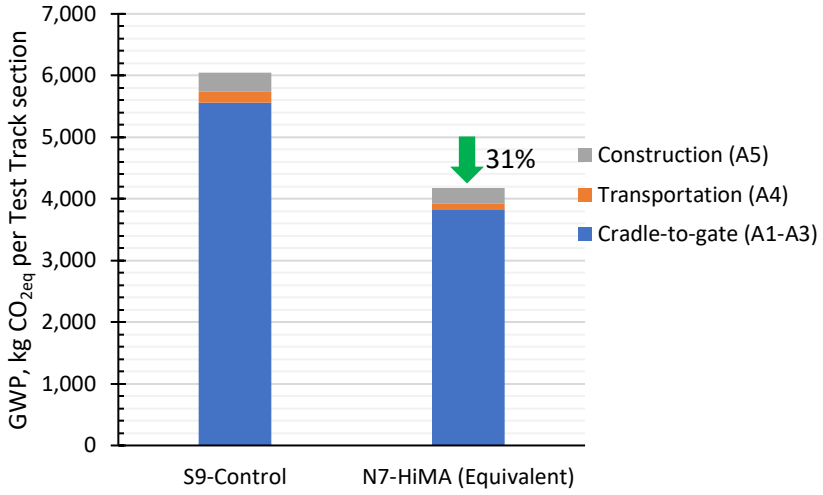

Figure 3.4 Cradle-to-Constructed Global Warming Potential of Section S9 and Structurally Equivalent Section N7

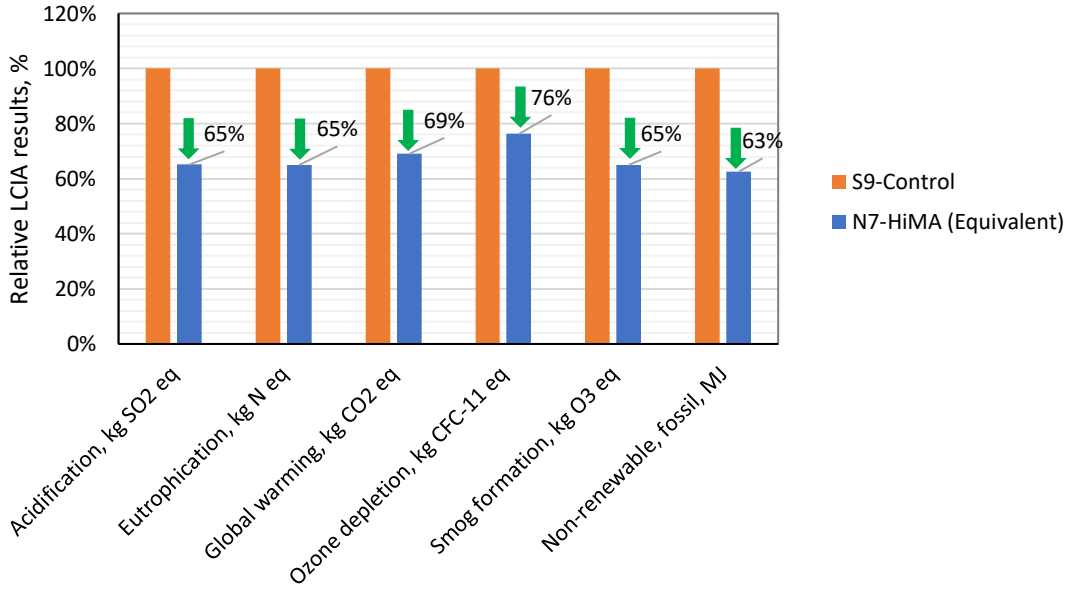

Figure 3.5 Cradle-to-Constructed Relative Environmental Impacts of Section S9 and Structurally Equivalent Section N7

3.5 CRADLE-TO-GRAVE

3.5.1 Maintenance and Rehabilitation Schedule

The system boundary of the LCA was further extended to include future maintenance and rehabilitation (M&R) activities for a cradle-to-grave LCA. The functional unit for the cradle-to-grave LCA was also selected as one lane-mile with an analysis period of 35 years of service life. It should be noted that Sections S9 and N7 were evaluated under controlled conditions at the Test Track, where no M&R activities were performed during the two-year trafficking period. To account for potential future M&R activities in the LCA, the AASHTO 1993 flexible pavement design equation (Equation 2.18) was used to predict the performance and future M&R activities of these two pavement cross sections as shown in Figure 3.6 and described in detailed below.

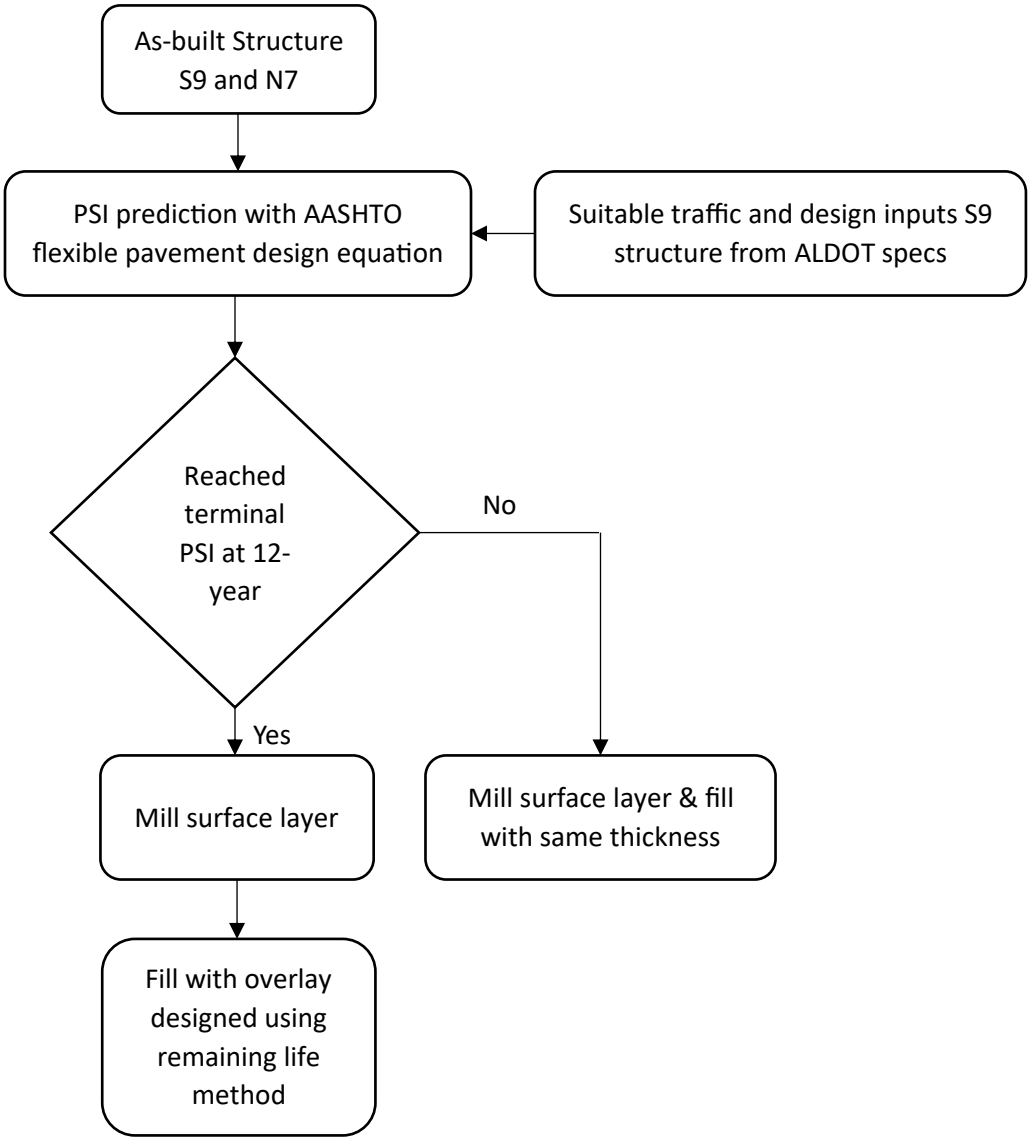

Figure 3.6 Methodology Used to Determine Future Maintenance and Rehabilitation Schedules

As previously mentioned, ALDOT uses a layer coefficient of 0.54 for conventional materials, such as unmodified or modified asphalt mixtures with typical polymer dosages. Given this structural coefficient for the surface, intermediate, and base layers, Section S9 has a structural number (SN) of 3.8, as shown in Figure 2.3. The backcalculated subgrade modulus for Section S9 averaged 26,160 psi, resulting in a corrected subgrade resilient modulus of 8,720 psi after applying a correction factor of 0.33 [28]. The backcalulated modulus of the granular base was 2,080 psi, which is considerably lower than typical granular layer moduli. Such a low modulus value for a granular base resulted in a negative structural coefficient when the relationship between the granular base structural coefficient and modulus was used from the AASHTO 1993 design guide [1]. Therefore, no structural contribution from the granular was assumed for Sections S9 and N7, and a value of zero for the structural coefficient of the granular base was used. Since the N7-HiMA section was constructed on the same subgrade and granular base as the S9 control section, the same foundation layer properties were assumed, including a corrected subgrade resilient modulus of 8,720 psi. With a layer coefficient of 0.92, as recommended in the earlier chapter for HiMA mixtures, the HiMA section (Section N7) would result in a structural number of 5.2, which is much higher than the control section.

In practice, a pavement section with S9's cross-section with a structural number of 3.8 and a subgrade resilient modulus of 8,720 psi would be designed and constructed on a two-lane rural highway with a traffic of 259,500 ESALs per year in both directions as per ALDOT pavement design guidelines [1]. As per ALDOT flexible pavement design guidelines, for a highway with 259,500 ESALs per year in both directions, the following design parameters would be used to imply the AASHTO 1993 design methodology.

- Reliability = 85%
- Z_R = -1.036
- S_0 = 0.49
- p_o = 4.2
- p_t = 3.0

The above design input values were used to predict the change in PSI over the analysis period for both the pavement sections on a two-lane rural highway with a traffic of 259,500 ESALs per year in both directions. As shown in Figure 3.7, the control section would reach the terminal serviceability (P_t) of 3.0 in 12 years due to the lower structural number of the section compared to the HiMA section. As the control section reaches the terminal serviceability (P_t) at the end of year 12, an overlay must be designed.

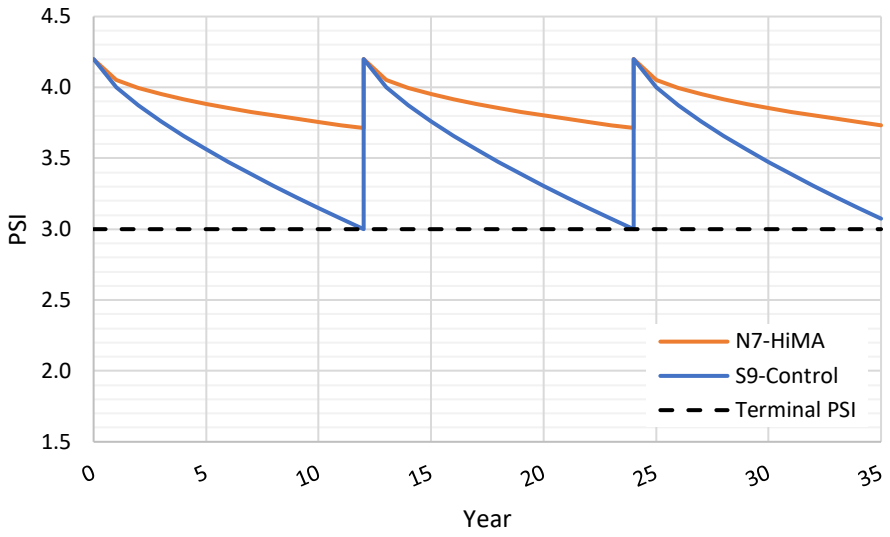

Figure 3.7 Cradle-to-Constructed Global Warming Potential of Sections S9 and N7

The required overlay thickness is a function of the structural number required for the future traffic demand and the effective structural number of the existing pavement after 12 years. The overlay was designed to sustain the traffic for another 12 years. A traffic growth value of 0% was assumed for simplicity purposes. Therefore, the required structural number for the future traffic demand would be the same as the initial structural number of the control section, which is 3.8. The remaining life method described in the AASHTO 1993 Design Guide was used to determine the effective structural number of the control section after 12 years of trafficking using Equation 3.3 [1].

$$RL = 100\left[1 - \left(\frac{N_p}{N_{1.5}}\right)\right] \quad \text{(Equation 3.3)}$$

Where:
RL = Remaining life, %
N_p = Total traffic to date, 18-kip ESAL
$N_{1.5}$ = Total traffic to pavement failure (to reach a P_t of 1.5), 18-kip ESAL

The remaining life of the control section after 12 years was estimated using total traffic after 12 years, which is 1,323,473 ESALs and total traffic the control section would sustain before reaching a terminal PSI of 1.5, calculated using Equation 3.2. The remaining life after 12 years was calculated to determine the condition factor of the control section using Figure 3.8 from the AASHTO 1993 overlay design procedure [1].

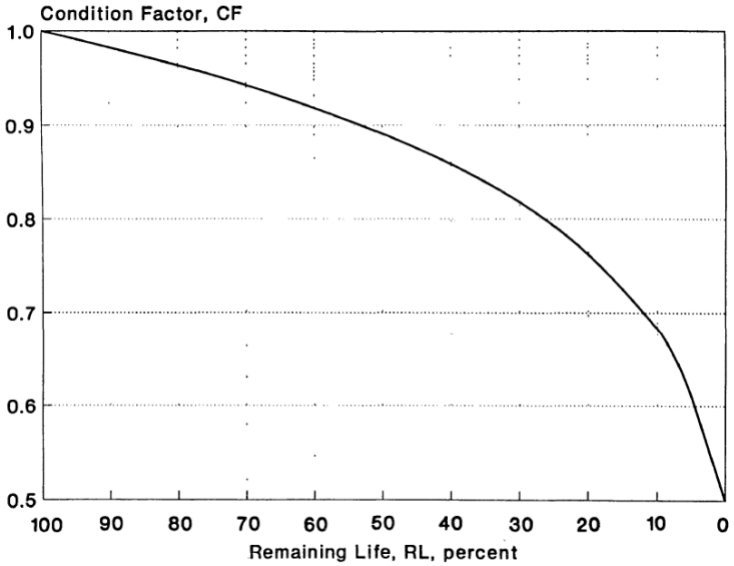

Figure 3.8 Relationship Between Condition Factor and Remaining Life [1].

The effective structural number of the control section after 12 years was calculated using Equation 3.4 with the initial structural number of the section and the condition factor determined from the earlier step. The effective structural numbers calculated for the control and HiMA sections are presented in Table 3.7.

$$SN_{eff} = CF \times SN_0 \quad \text{(Equation 3.4)}$$

Where:
SN_{eff} = Effective structural number of the pavement after N_p ESALs, in.
SN_0 = Initial structural number of the pavement, in.
CF = Condition factor

Table 3.7 Remaining Life and Effective Structural Number of Control and HiMA Sections

Section	Year	N_p	$N_{1.5}$	RL	CF	SN_{eff}
Control	0	-	4,080,710	-	-	3.80
	12	1,323,473		68%	0.934	3.53
	24	1,323,473		68%	0.934	3.53
HiMA	0	-	45,659,834	-	-	5.20
	12	1,323,473		97%	0.988	5.14
	24	1,323,473		97%	0.988	5.14

The maintenance activity for the control section is assumed to be mill and fill of the surface layer in year 12. The effective structural number of the milled surface layer was calculated using the condition factor determined earlier and the thickness of the milled surface layer, which is 1.2 inches, as shown in Equation 3.5. Equations 3.6 and 3.7 were employed to determine the overlay thickness needed for the

mill and fill operation in year 12. The same procedure was repeated to determine the overlay thickness needed for the mill and fill operation at year 24 of the analysis period.

$$SN_{mill} = 0.54 \times CF \times D_1 \quad \text{(Equation 3.5)}$$

$$SN_{OL} = SN_f - \left[SN_{eff} - SN_{mill}\right] \quad \text{(Equation 3.6)}$$

$$D_{OL} = \frac{SN_{0L}}{a_{0L}} \quad \text{(Equation 3.7)}$$

Where:
SN_{mill} = Effective structural number of the milled surface layer after 12 years of trafficking, in.
SN_{eff} = Effective structural number of the existing pavement prior to milling, in.
D_1 = Milled surface layer thickness, in.
CF = Condition factor after 12 years of trafficking
SN_f = Required structural number for carrying future traffic, in.
SN_{OL} = Required overlay structural number, in.
a_{ol} = Structural coefficient of the overlay, which is 0.54 for the control, and 0.92 for HiMA mixtures

From Figure 3.7, the HiMA section showed no significant reduction in the PSI values and did not reach the terminal PSI of 3.0 after 35 years of analysis period due to its high initial structural number. Even though the HiMA section did not reach terminal PSI in years 12 and 24, a periodic mill and fill of surface layer activity was assumed at years 12 and 24 for the HiMA section. Table 3.8 presents the future M&R schedule for the control and HiMA sections determined following the AASHTO 1993 flexible pavement design guidelines.

Table 3.8 Maintenance and Rehabilitation Schedule for Control and HiMA Sections

Year	Activity	
	Control	HiMA
0	Initial construction	Initial construction
12	1.2” mill and 1.6” fill	1.0” mill and 1.0” fill
24	1.6” mill and 2.0” fill	1.0” mill and 1.0” fill
35	end-of-analysis period	end-of-analysis period

3.5.2 Cradle-to-Grave LCA Results

The M&R schedule presented in Table 3.8 was used to conduct a cradle-to-grave LCA of control and HiMA sections, following the methodology explained earlier. The functional unit for this assessment is one lane-mile, with both sections carrying the same traffic under identical environmental conditions for a 35-year analysis period. Figure 3.9 displays the cradle-to-grave GWP of the control and HiMA pavement sections, taking into account future maintenance and repair activities.

From Figure 3.9, the initial construction stage (A1-A5) had a significant impact on the cradle-to-grave emissions. However, future M&R stages (B2-B5) contributed about 25-35% of the overall GWP. The as-built cradle-to-constructed LCA results showed that the HiMA section had 9% lower GWP compared to the control section, as shown in Figure 3.1. This reduction increased to 18% once the system boundary

was extended to include future M&R activities. The further reduction in GWP is primarily due to the higher structural number and better performance of the HiMA section, which does not require additional overlay thickness for the M&R activities at years 12 and 24 of the analysis period.

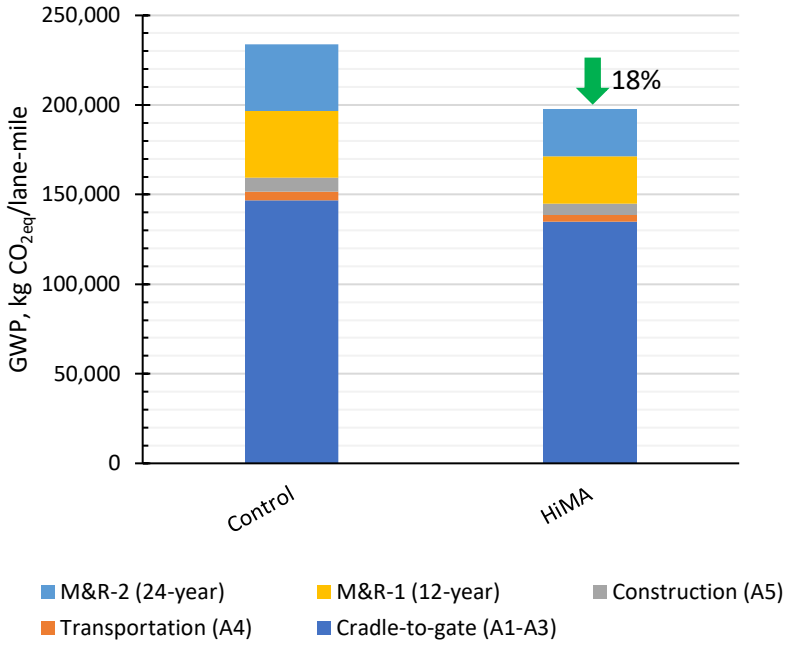

Figure 3.9 Cradle-to-Grave Global Warming Potential of Control and HiMA sections

Figure 3.10 presents the cradle-to-grave relative environmental impacts of control and HiMA sections. The relative LCIA results indicate that the HiMA section has a 13 to 25% reduction in impact indicators compared to the control section with conventional asphalt mixtures.

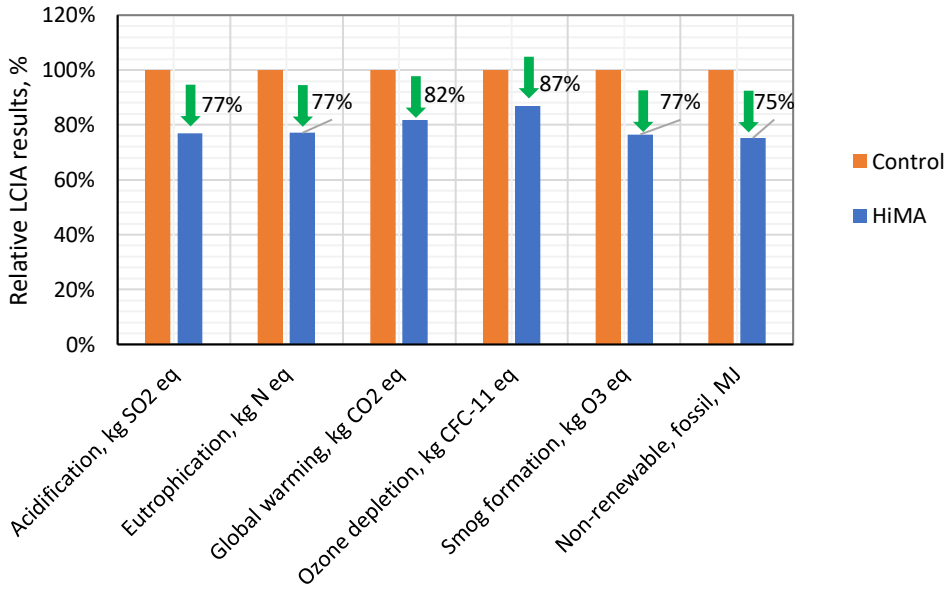

Figure 3.10 Cradle-to-Grave Relative Environmental Impacts of Control and HiMA Sections

3.5.2 Sensitivity Analysis

As shown in Figure 3.7, the HiMA section only reached a PSI of 3.8 in 35-years, which is well over the terminal PSI of 3.0. The as-built HiMA section reaches a terminal PSI of 3.0 in 155 years due to very high structural number resulted from HiMA's structural layer coefficient of 0.92. Even though the HiMA section did not reach terminal PSI, a routine maintenance activity of surface layer mill and fill was used in the earlier analysis to be more conservative. However, in practice, a highway agency does not do mill and fill maintenance activity unless the pavement section reaches the terminal PSI. Therefore, a sensitivity analysis was conducted in this section to assess the impact of having longer maintenance cycles of 14, 16, 18 years, and "no M&R" for the HiMA section on the full life cycle of environmental impacts. Table 3.8 presents the future M&R schedule for the control and HiMA sections with different maintenance cycles of 14, 16, 18 years, and "no M&R" for the HiMA section.

Table 3.9 Future Maintenance and Rehabilitation Schedule for Control and HiMA Sections with Different Maintenance Cycles

	Activity					
Year	**Control**	**HiMA 12 year**	**HiMA 14 year**	**HiMA 16 year**	**HiMA 18 year**	**HiMA "No M&R"**
0	Initial Construction					
12	1.2" mill & 1.6" fill	1.0" mill & fill				
14			1.0" mill & fill			
16				1.0" mill & fill		
18					1.0" mill & fill	
24	1.6" mill & 2.0" fill	1.0" mill & fill				
28			1.0" mill & fill			
32				1.0" mill & fill		
35	end-of-analysis period					

Figure 3.11 presents the results of the sensitivity analysis in terms of cradle-to-grave GWP emissions of control and HiMA sections. The scenarios of 12-, 14-, and 16-year maintenance cycles for the HiMA section resulted in an 18% reduction in GWP. The reason for the same percent reduction in GWP emissions for different maintenance cycles is that the LCA framework does not give any credit to the remaining life of the pavement beyond the analysis period as salvage value in a LCCA framework. The 18-year maintenance cycle for the HiMA section resulted in a 29% reduction in GWP compared to the control section, as the HiMA section required only one maintenance activity during the 35-year analysis

period. The “no M&R” scenario for the HiMA section resulted in a 40% reduction in GWP compared to the control section.

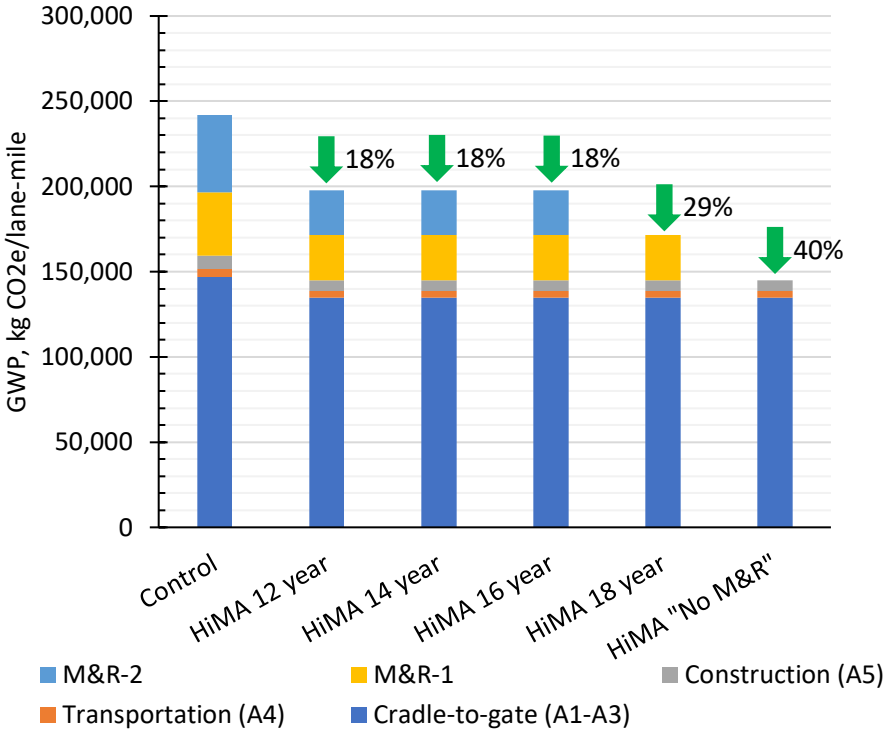

Figure 3.11 Cradle-to-Grave Global Warming Potential of Control and HiMA sections with different maintenance cycles

3.6 SUMMARY & CONCLUSIONS

The objective of this chapter was to conduct a comparative LCA between two pavement sections that were built at the NCAT Test Track in 2009, one with conventional asphalt mixtures and the other with HiMA mixtures. The comparative LCA aimed at quantifying differences in key environmental impacts between the two pavement cross sections. Initially, a cradle-to-constructed system boundary was considered for the quantification of the comparative LCA. However, the as-built HiMA section outperformed the control section after 20 million ESAL load applications. Therefore, two approaches were used to perform a reasonable LCA comparison between the two cross sections. First, a structural equivalent thickness approach was utilized to determine the thickness of the HiMA section required to be structurally equivalent to the as-built control section. Second, the system boundary was extended to include future maintenance and rehabilitation activities, taking the performance differences between the two sections into account. Based on the results of this chapter, the following conclusions and recommendations are made:

1. The production (cradle-to-gate, A-A3) of HiMA asphalt mixtures used for surface, intermediate, and base layers for Section N7 resulted in 15, 9, and 12% higher GWP emissions compared to conventional asphalt mixtures used for Section S9, respectively.

2. From a cradle-to-constructed (A1-A5) system boundary using as-built cross sections, it was found that the GWP emissions for the HiMA section (N7) using HiMA mixtures had 9% lower GWP emissions compared to the control section (S9) with conventional asphalt mixtures. The HiMA section resulted in a 3 to 17% reduction in other LCIA indicators considered in the study (e.g., acidification, eutrophication, etc.).
3. The equivalent thickness approach, which ensures structural equivalency between HiMA and control sections, resulted in 31% lower cradle-to-constructed (A1-A5) GWP emissions for the HiMA section compared to the control section. The HiMA section resulted in a 24 to 37% reduction in other LCIA indicators considered in the study.
4. The AASHTO 1993 pavement design method was used to extend the system boundary of LCA to include future maintenance and rehabilitation activities of as-built HiMA and control sections. The cradle-to-grave LCA analysis resulted in 18% lower GWP emissions for section the HiMA section compared to the control. The HiMA section resulted in a 13 to 18% reduction in other LCIA indicators considered in the study.
5. The sensitivity analysis results revealed that a reduction in GWP emissions as high as 29% is possible with an extended maintenance cycle of 18 years for the HiMA section.

CHAPTER 4: SUMMARY, CONCLUSIONS & RECOMMENDATIONS

The objective of this study was to recalibrate the structural coefficient for HiMA mixtures to be used in the 1993 AASHTO Design Guide for flexible pavements and to perform a comparative Life Cycle Assessment (LCA) of two pavement sections constructed with HiMA and conventional mixtures at the NCAT Test Track in 2009. For the recalibration effort, data from three different sets of test sections at the NCAT Test Track were used, in conjunction with four different computational methodologies, to determine a range of structural coefficients.

For the comparative LCA analysis, initially, a cradle-to-constructed system boundary was considered for the quantification. However, the as-built HiMA section outperformed the control section after 20 million ESAL load applications. Therefore, two approaches were used to perform a reasonable LCA comparison between the two cross sections: (1) a structural equivalent thickness approach, and (2) the system boundary was extended to include future maintenance and rehabilitation activities, taking the performance differences between the two sections into account. Based on the results of the study, the following conclusions and recommendations are made:

4.1 STRUCTURAL COEFFICIENT OF HiMA MIXTURES

- Methods that relied only on computing structural coefficients from in situ material properties determined through FWD testing and backcalculation (i.e., SN_{eff} and Modulus Correlation) did not distinguish the HiMA sections from the control sections. This was expected since these methods essentially assume the same performance characteristics for a given asphalt concrete modulus.
- The Equivalent Sections approach, used with the 2009 sections, considered both the in-situ strain measurements and laboratory fatigue performance data distinguished between the HiMA and control AC materials. Values from 0.71 to 0.96 for HiMA were computed, depending on how the data were grouped and what was assumed for the control structural coefficient (0.44 or 0.54). Recommended values from these sections were 0.75 and 0.92, corresponding to control structural coefficients of 0.44 and 0.54, respectively.
- Calibrating to performance data, which was only possible with the 2010 rehabilitation section, resulted in 0.92 for the HiMA structural coefficient. This result was identical to the 0.92 found from the Equivalent Sections approach with the 2009 sections when 0.54 was assumed for the control material.
- Since both approaches that considered performance resulted in 0.92, it is recommended to use a_{HiMA} = 0.92 when 0.54 would be assigned to conventional materials (i.e., either unmodified or modified at typical polymer contents). To be conservative, it is recommended to use a_{HiMA} = 0.75 if conventional materials would have 0.44 for their structural coefficient.

4.2 LIFE CYCLE ASSESSMENT OF HiMA PAVEMENT SECTION

- The production (cradle-to-gate, A-A3) of HiMA asphalt mixtures used for surface, intermediate, and base layers for Section N7 resulted in 15, 9, and 12% higher GWP emissions compared to conventional asphalt mixtures used for Section S9, respectively.
- From a cradle-to-constructed (A1-A5) system boundary using as-built cross sections, it was found that the GWP emissions for the HiMA section (N7) using HiMA mixtures had 9% lower GWP emissions compared to the control section (S9) with conventional asphalt mixtures. The HiMA section resulted

in a 3 to 17% reduction in other LCIA indicators considered in the study (e.g., acidification, eutrophication, etc.), presented in Table 4.1.

- The equivalent thickness approach, which ensures structural equivalency between HiMA and control sections, resulted in 31% lower cradle-to-constructed (A1-A5) GWP emissions for the HiMA section compared to the control section. The HiMA section resulted in a 24 to 37% reduction in other LCIA indicators considered in the study, presented in Table 4.1.
- The AASHTO 1993 pavement design method was used to extend the system boundary of LCA to include future maintenance and rehabilitation activities of as-built HiMA and control sections. The cradle-to-grave LCA analysis resulted in 18% lower GWP emissions for section the HiMA section compared to the control. The HiMA section resulted in a 13 to 18% reduction in other LCIA indicators considered in the study, presented in Table 4.1.
- The sensitivity analysis results concluded that a reduction in GWP emissions as high as 29% is possible with an extended maintenance cycle of 18 years for the HiMA section.

Table 4.1 Percent Reduction in Environmental Impacts of Using HiMA Mixtures

Impact Indicator	**Cradle-to-Constructed (A1-A5)**		**Cradle-to-Grave (A1-A5 + B2-B5)**
	As built	*Equivalent Thickness*	*Equivalent Performance*
Acidification	15%	35%	23%
Eutrophication	14%	35%	23%
Global warming	9%	31%	18%
Ozone depletion	3%	24%	13%
Smog formation	15%	35%	23%
Non-renewable, fossil	17%	37%	25%

REFERENCES

1. American Association of State and Highway Transportation Officials. *AASHTO Guide for Design of Pavement Structures*. Washington D.C., 1993.
2. Highway Research Board (HRB). *The AASHO Road Test, Report 5*. Pavement Research Special Report 61E, National Academy of Sciences – National Research Council, Washington, DC, 1962.
3. Timm, D.H., M.M. Robbins, N. Tran and C. Rodezno. *Recalibration Procedures for the Structural Asphalt Layer Coefficient in the 1993 AASHTO Pavement Design Guide.* Report No. 14-08, National Center for Asphalt Technology, Auburn University, 2014.
4. Peters-Davis, K. and D.H. Timm. *Recalibration of the Asphalt Layer Coefficient.* Report No. 09-03, National Center for Asphalt Technology, Auburn University, 2009.
5. Timm, D.H., M.M. Robbins, J.R. Willis and A.J. Taylor. *Field and Laboratory Study of High-Polymer Mixtures at the NCAT Test Track: Final Report*. Report No. 13-03, National Center for Asphalt Technology, Auburn University, 2013.
6. Timm, D.H., M.M. Robbins, J.R. Willis, N. Tran and A.J. Taylor. *Field and Laboratory Study of High-Polymer Mixtures at the NCAT Test Track: Interim Report*. Report No. 12-08, National Center for Asphalt Technology, Auburn University, 2012.
7. Timm, D.H., R. Powell, J.R. Willis and R. Kluttz. Pavement Rehabilitation Using High Polymer Asphalt Mix. *Proceedings of the 91st Annual Transportation Research Board*, Washington, D.C., 2012.
8. Timm, D.H. *Design, Construction, and Instrumentation of the 2006 Test Track Structural Study*. Report No. 09-01, National Center for Asphalt Technology, Auburn University, 2009.
9. Taylor, A.J. and D.H. Timm. *Mechanistic Characterization of Resilient Moduli for Unbound Pavement Layer Materials*. Report No. 09-06, National Center for Asphalt Technology, Auburn University, 2009.
10. Timm, D.H., D. Gierhart and J.R. Willis. Strain Regimes Measured in Two Full Scale Perpetual Pavements. *Proceedings, International Conference on Perpetual Pavements*, Columbus, Ohio, 2009.
11. West, R.C., D.H. Timm, B. Powell, M. Heitzman, N. Tran, C. Rodezno, D. Watson, F. Leiva and A. Vargas, *Phase VI (2015-2018) NCAT Test Track Findings*. NCAT Report 18-04, National Center for Asphalt Technology, Auburn University, 2019.
12. Timm, D.H., A. Vargas-Nordcbeck. Structural Coefficient of Open Graded Friction Course. *Transportation Research Record 2305*, Transportation Research Board, 2012, pp. 102-110.
13. Al-Omari, B. and M.I. Darter. Relationships between International Roughness Index and Present Serviceability Rating. *Transportation Research Record 1435*, Transportation Research Board, Washington, D.C. 1994, pp. 130-136, 1994.
14. ISO 14044. Environmental management. *Life cycle assessment. Requirements and guidelines*. International Organization for Standardization, First edition, Geneva, 2006.
15. West, R., N. Tran, M. Musselman, J. Skolnik and M. Brooks. *A Review of the Alabama Department of Transportation's Policies and Procedures for Life Cycle Cost Analysis for Pavement Type Selection*. NCAT, Report 13-06. Auburn, AL, 2013.
16. Musselman, J., and R. West. *Life Cycle Cost Analysis–End of Life Considerations*. NCAT Report 20-05. Auburn, AL, 2020.
17. Bare, J., D. Young, S. Qam, M. Hopton and S. Chief. *Tool for the Reduction and Assessment of Chemical and other Environmental Impacts (TRACI)*. US Environmental Protection Agency, Washington, DC, 2012.

18. Gürzenich, D., J. Mathur, N. Bansal, and H. Wagner. Cumulative energy demand for selected renewable energy technologies. *The International Journal of Life Cycle Assessment*, 4, pp.143-149, 1999.
19. Mukherjee, A., C. Bhat and J. Harvey. *Challenges in meeting data needs for use of environmental product declarations in pavement design and construction: State of practice and future scope*. (No. FHWA-HRT-20-022). United States. Federal Highway Administration. Office of Infrastructure Research and Development, 2020.
20. Wildnauer, M., E. Mulholland and J. Liddie. *Life cycle assessment of asphalt binder*. Asphalt Institute, Lexington, Kentucky, 2019.
21. Asphalt Institute. *Life Cycle Assessment of Styrene-Butadiene-Styrene Block Copolymer.* Asphalt Institute, Lexington, Kentucky, 2022.
22. Mukherjee, A. *Update to the Life Cycle Assessment for Asphalt Mixtures in Support of the Emerald Eco Label Environmental Product Declaration Program*. National Asphalt Pavement Association, Greenbelt, Maryland, 2021.
23. Marceau, M., A. Nisbet and G. Van Geem. *Life Cycle Inventory of Portland Cement Concrete*. Portland Cement Association, 2007.
24. National Asphalt Pavement Association (NAPA). *Product Category Rules (PCR) for Asphalt Mixtures*. Lanham, Maryland, 2022.
25. National Renewable Energy Laboratory (NREL). *USLCI Quarterly Release: Fall 2022 Update*. USLCI 2022 Q2 v1, 2021.
26. Salehi, S., M. Arashpour, J. Kodikara and R. Guppy Comparative Life Cycle Assessment of Reprocessed Plastics and Commercial Polymer Modified Asphalts. *Journal of Cleaner Production*, 337, 130464, 2022.
27. Couhape L., M. Angelone, P. Raffaelli, O. Martinez, M. Zorzutti and J. Reano. Comparative Study of Mechanistic-empirical Structural Design Methods Applied to Sustainable Asphalt Mixtures. *The Open Transportation Journal*, 18(1), 2024.
28. Tran, N., M. Robbins, D. Timm, R. Willis and C. Rodezno. *Refined Limiting Strain Criteria and Approximate Ranges of Maximum Thicknesses for Designing Long--Life Asphalt Pavements* NCAT Report 15-05R, Auburn, AL, 2016.